Flow characteristics and dispersion during drug delivery in a permeable microvessel

By

Godfrey Bashaga

Reg No. 12001181

A thesis submitted to faculty of science in partial fulfilment of the requirements for the award of the degree of master of science in pure and applied mathematics

Supervisor: Prof Sachin Shaw

e-mail: shaws@biust.ac.bw

Department of Mathematics and Statistical Sciences

October 21, 2020

Flow characteristics and dispersion during drug delivery in a permeable microvessel

BY

GODFREY BASHAGA

Reg. No:12001181

BSc Applied Mathematics, Botswana International University of science and Technology

Department of Mathematics and Statistical Sciences

Faculty of Sciences

Botswana International University of Science and Technology

E-mail: godfrey.bashaga@studentmail.biust.ac.bw

A Thesis Submitted to the Faculty of Sciences in Partial Fulfillment of the Requirement for the Award of the Degree of Master of Science in Pure and Applied Mathematics of BIUST

Supervisor:

Dr Sachin Shaw

Department of Mathematics

and Statistical Sciences

Faculty of Sciences, BIUST

Email: shaws@biust.ac.bw

Signature:..... Date: 21/10/2020

Declaration

I **Godfrey Bashaga** submitting this thesis/dissertation, declare that the entirety of the work contained therein is my own, original work, that I am the sole author thereof (save to the extent explicitly otherwise stated), that reproduction and publication thereof by Botswana International University of Science and Technology will not infringe any third party rights and that I have not previously in its entirety or in part submitted it for obtaining any qualification.

Signature:.....

Date:.....21/10/2020.....

Certification

The undersigned certifies that he has read and hereby recommends for acceptance by the Faculty of Science a thesis titled: Flow characteristics and dispersion during drug delivery in a permeable microvessel, in fulfillment of the requirements for the Msc Degree in Pure and Applied Mathematics of BIUST.

Student:

Godfrey Bashaga

Email: godfrey.bashaga@studentmail.biust.ac.bw

Signature:.....

Date:.....21/10/2020.....

Supervisor:

Dr Sachin Shaw

Email: shaws@biust.ac.bw

Signature:.....

Date:.....21/10/2020.....

Acknowledgement

I would like to thank my supervisor , Dr Sachin Shaw for the time and support he invested in helping me to complete this Thesis. I would like to thank Botswana International University of Science and Technology (BIUST) and Simons foundation for the support they gave me through out my Masters. My deepest regards to my Parents for their blessings, affection and continuous support. Also, Last but not the least, I thank God, the Almighty for giving me the inner willingness, strength and wisdom to carry out this research work successfully.

Abstract

Understanding how fluid flow and how solutes disperse in human bodies is crucial in Biomedical Engineering. The study of blood rheology is critical as it may help in detecting, designing a treatment for some blood related diseases and understanding them better. The aims of the present thesis is to study the effect of rheological parameters on blood flow and solute dispersion in a microvessel. Firstly the impact of stress jump condition and heterogeneous reaction on velocity, temperature and concentration during Casson fluid flow through a permeable microvessel was analysed by taking the flow to be steady. We have used a two phase model where the radius of the microvessel is divided into two parts. The flow nature at the clear region is defined by non-Newtonian Casson fluid and the peripheral region is defined by Newtonian fluid. The wall of the microvessel is considered as permeable and the nature defined by Brinkman model. Secondly we analyze steady solute dispersion in Herschel-Bulkely fluid in a permeable microvessel. Due to the aggregation of red blood cells at the axial in the vessel, we have continued the two phase model. Blood in the peripheral region is taken to obey Newtonian fluid character while at the clear region obeys the non-Newtonian Herschel-Bulkely fluid character. Nature of the microvessel's inner wall is considered to be permeable and characterised by Darcy model. The effect of blood rheological parameter, permeability parameter, pressure constant, particle volume fraction, stress jump constant, slip constant and yield stress on the process are analysed and discussed. Lastly we analyze unsteady dispersion in Herschel-Bulkely fluid through a mild stenosed artery and looking at the pulsatile flow of blood under the influence of body acceleration.

Contents

Chapter 1

Introduction

1.1 Basic introduction

Fluid Dynamics is the study of fluids at rest and in motion. Branching from fluid dynamics, Bio-fluid dynamics is a fascinating study which has attracted the attention of researchers and the general public for years as it is directed towards finding solutions to some of the human body related diseases and disorders. Understanding the concept of human body fluid dynamics is difficult owing to the fact that in vivo experiments are not easy to undertake. Both theoretical and computational biofluid dynamics play a major role in the comprehension of human body biofluid dynamics.

1.1.1 Viscosity

Viscosity is the measure of how fluids can deform under the action of a shear force. In simple terms it is the stickiness of a fluid. Viscosity is denoted by the symbol μ, It relates to viscous shear stress τ, viscosity μ and shear rate $\frac{\partial u}{\partial y}$, hence Newton's law of viscosity.

$$\tau = \mu \frac{\partial u}{\partial y}. \tag{1.1}$$

1.1.2 Kinematic Viscosity

Kinematic viscosity is given as the ratio of dynamic viscosity to mass density (denoted by ν)

$$\nu = \mu/\rho, \tag{1.2}$$

where ρ is the density of the fluid and μ is dynamic viscosity.

1.2 Bio-Fluid Dynamics Equations

This section introduces governing equations for solid deformation and fluid motion, which are the basic equations that describe flow, these are continuity equation, momentum equation, energy equation and concentration equation.

1.2.1 Continuity Equation

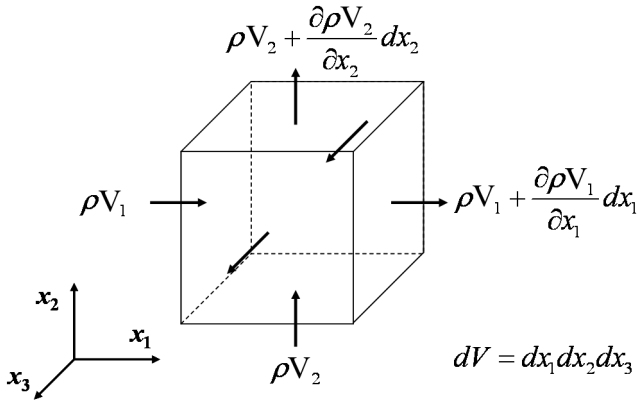

Figure 1.1: Continuity equation in control volume (www.continuummechanics.org)

The foundation of the conservation mass principle for fluid dynamics is that the fluid mass can neither be created nor destroyed within the system of interest. According to Clement et al. (2006) when using the conservation of mass concept, one should consider a cube in Fig. 1.1 above which is of the dimensions $dx_1 dx_2 dx_3$. The continuity equation can be derived by adding the rate at which mass is flowing in and out of the control volume(the cube), where net flow is equal to the rate of change of mass within it. Equating all the net rate mass flux in and out of the control volume we get

$$\frac{\partial}{\partial t}(\rho dx_1 dx_2 dx_3) \quad = \rho v_1 (dx_2 dx_3) + \rho v_2 (dx_1 dx_3) + \rho v_3 (dx_1 dx_2)$$

$$-\left(\rho v_1 + \frac{\partial \rho v_1}{\partial x_1} dx_1\right) dx_2 dx_3 - \left(\rho v_2 + \frac{\partial \rho v_2}{\partial x_2} dx_2\right) dx_1 dx_3 - \left(\rho v_3 + \frac{\partial \rho v_3}{\partial x_3} dx\right) dx_1 dx_2. \quad (1.3)$$

Then cancelling terms and diving through by $dx_1dx_2dx_3$ gives the continuity equation

$$\frac{\partial \rho v_1}{\partial x_1} + \frac{\partial \rho v_2}{\partial x_2} + \frac{\partial \rho v_3}{\partial x_3} = -\frac{\partial \rho}{\partial t}. \tag{1.4}$$

In cylindrical coordinates is given as

$$-\frac{\partial \rho}{\partial t} = \frac{1}{r}\frac{\partial}{\partial r}(r\rho v_r) + \frac{1}{r}\frac{\partial}{\partial r}(r\rho v_\theta) + \frac{\partial \rho v_z}{\partial z}. \tag{1.5}$$

1.2.2 Momentum Equation

Using the same control volume in Fig. 1.1, we derive the momentum equation based on Newton's law, for moving fluids. The general form of the momentum equation in cartesion coordinates($(x_1, x_2, x_3) = (x, y, z)$) are as given below

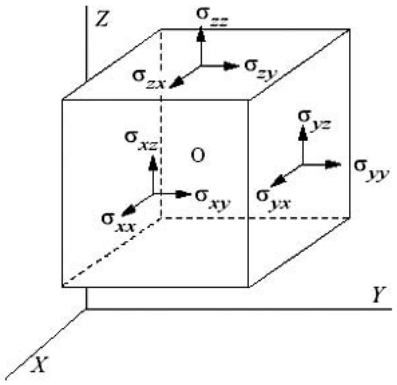

Figure 1.2: Notation for stresses(www.iue.tuwien.ac)

$$\rho\left(\frac{\partial v_1}{\partial t} + v_1\frac{\partial v_1}{\partial x} + v_2\frac{\partial v_1}{\partial y} + v_3\frac{\partial v_1}{\partial z}\right) = \rho B_x - \frac{\partial p}{\partial x} + \frac{\partial \sigma_{xx}}{\partial x} + \frac{\partial \sigma_{xy}}{\partial y} + \frac{\partial \sigma_{xz}}{\partial z}, \tag{1.6}$$

$$\rho\left(\frac{\partial v_2}{\partial t} + v_1\frac{\partial v_2}{\partial x} + v_2\frac{\partial v_2}{\partial y} + v_3\frac{\partial v_2}{\partial z}\right) = \rho B_y - \frac{\partial p}{\partial y} + \frac{\partial \sigma_{yx}}{\partial x} + \frac{\partial \sigma_{yy}}{\partial y} + \frac{\partial \sigma_{yz}}{\partial z}, \tag{1.7}$$

$$\rho\left(\frac{\partial v_3}{\partial t} + v_1\frac{\partial v_3}{\partial x} + v_2\frac{\partial v_3}{\partial y} + v_3\frac{\partial v_3}{\partial z}\right) = \rho B_z - \frac{\partial p}{\partial z} + \frac{\partial \sigma_{zx}}{\partial x} + \frac{\partial \sigma_{zy}}{\partial y} + \frac{\partial \sigma_{zz}}{\partial z}, \tag{1.8}$$

where B_i is the body force and σ_{ij} are the shear stress given in the cube in Fig. 2.2

Since in Biofluid dynamics we deal with incompressible fluid flow, the basic governing equations are given as follows (changing the stresses to velocities)

$$\rho\left(\frac{\partial v_1}{\partial t}+v_1\frac{\partial v_1}{\partial x}+v_2\frac{\partial v_1}{\partial y}+v_3\frac{\partial v_1}{\partial z}\right)=\rho B_x-\frac{\partial p}{\partial x}+\mu\left(\frac{\partial^2 v_1}{\partial x^2}+\frac{\partial^2 v_1}{\partial y^2}+\frac{\partial^2 v_1}{\partial z^2}\right), \tag{1.9}$$

$$\rho\left(\frac{\partial v_2}{\partial t}+v_1\frac{\partial v_2}{\partial x}+v_2\frac{\partial v_2}{\partial y}+v_3\frac{\partial v_2}{\partial z}\right)=\rho B_y-\frac{\partial p}{\partial y}+\mu\left(\frac{\partial^2 v_2}{\partial x^2}+\frac{\partial^2 v_2}{\partial y^2}+\frac{\partial^2 v_2}{\partial z^2}\right), \tag{1.10}$$

$$\rho\left(\frac{\partial v_3}{\partial t}+v_1\frac{\partial v_3}{\partial x}+v_2\frac{\partial v_3}{\partial y}+v_3\frac{\partial v_3}{\partial z}\right)=\rho B_z-\frac{\partial p}{\partial z}+\mu\left(\frac{\partial^2 v_3}{\partial x^2}+\frac{\partial^2 v_3}{\partial y^2}+\frac{\partial^2 v_3}{\partial z^2}\right), \tag{1.11}$$

1.2.3 Concentration Equation

The general equation of concentration in cartesian coordinates

$$\frac{\partial C}{\partial t}+v_1\frac{\partial C}{\partial x}+v_2\frac{\partial C}{\partial y}+v_3\frac{\partial C}{\partial z}=D_m\left(\frac{\partial^2 C}{\partial x^2}+\frac{\partial^2 C}{\partial y^2}+\frac{\partial^2 C}{\partial z^2}\right), \tag{1.12}$$

1.2.4 Temperature Equation

The general equation of temperature in cartesian coordinates:

$$\frac{\partial T}{\partial t}+v_1\frac{\partial T}{\partial x}+v_2\frac{\partial T}{\partial y}+v_3\frac{\partial T}{\partial z}=\alpha\left(\frac{\partial^2 T}{\partial x^2}+\frac{\partial^2 T}{\partial y^2}+\frac{\partial^2 T}{\partial z^2}\right), \tag{1.13}$$

where $\alpha = k/\delta C_p$.

1.3 Boundary Condition

Every Boundary value problem (differential equation) has to have boundary conditions (restrictions). Boundary conditions are divided into three types namely Dirichlet boundary condition, Neumann boundary condition and Mixed boundary condition.

1.3.1 Dirichlet Boundary Condition

Dirichlet boundary condition specifies the value that the unknown function needs to take on along the boundary of the domain, For example slip condition specifies that the velocity of a fluid at the wall of the channel is non-zero at the wall and no slip condition specifies that that at the wall the velocity is equal to zero.

1.3.2 Neumann Boundary Condition

Neumann boundary condition specifies that the derivative of the variable is normal to the boundary hence it is called fixed gradient e.g $\partial u/\partial r = 0$ at $r = r_p$.

1.3.3 Mixed Boundary Condition

Mixed boundary condition is a combination of the Dirichlet boundary condition and Neumann boundary condition, consisting of linear/ non-linear combination of the values of the field. Its derivatives on the boundary, for example

$$\frac{\partial u_1}{\partial r} = \mu_2 \left(\frac{\partial u_2}{\partial r} - \beta u_2 \right) \quad \text{at} \quad r = h_1,$$

which explains the stress jump condition at the interface of two regions.

1.4 Blood Rheology

1.4.1 General Introduction

Blood is a complex body fluid (liquid tissue) consisting of several formed elements (cells) suspended in an aqueous fluid matrix (plasma). Most human adults have $4 - 6$ litres of blood.

1.4.2 Structure of Blood

Plasma (50% to 60% of blood)

Is yellowish water like part of blood containing dissolved foods substances(nutrients) and other substances e.g O_2, CO_2 etc.

Formed elements ($\approx 45\%$ of blood)

- Red Blood Cell (erythrocytes)-Responsible for carrying oxygen around the body.
- White Blood Cell (leukocytes)-Responsible for human immune response.
- Platelets-Responsible for blood clotting.

1.4.3 Blood Vessel Structure

Blood vessels are channels of blood transportation in human bodies. Blood vessels are divided into three groups;

- Arteries- They transport blood to all parts of the body from the heart.
- Capillaries- Smallest blood vessels, they covey blood between arterioles and venules.
- Veins- They transport blood to the heart from different parts of the body.

1.5 Bio-Fluid Flow Models

Blood flows in different ways depending on the channel it is flowing in. The flow can be in a closed circulatory system (arteries, veins, capillaries) or an open circulatory system (heart etc). Nanda and Basun Mallik [25] pointed out that blood behaves like Newtonian fluids in large blood vessels it while in narrow blood vessels behaves like Non-Newtonian fluids (Casson, Herschely-Bulkely, Power law and Bingham fluids). The following, Table 1.1 and Fig. 1.3 demonstrates the behaviour, the types of fluids and models that define the fluids

Table 1.1: Types of fluids and models

Fluid	Model
Newtonian	$\tau = \eta\dot{\gamma}$
Pseudoplastic(Power law)	$\tau = k\dot{\gamma}n < 1$
Dilatant(Power law)	$\tau = k\dot{\gamma}n > 1$
Bingham	$\tau = \tau_y + \eta\dot{\gamma}^n$
Casson	$\tau^{1/2} = \tau_y^{1/2} + \eta\dot{\gamma}^{1/2}$
Herschel-Bulkely(Yield pseodoplastic)	$\tau = \tau_y + k\dot{\gamma}^n$

where τ = shear stress, $\dot{\gamma}$ = shear rate, η = apparent viscosity, k = consistency index, n = flow behaviour index.

1.5.1 Two Phase Flow Model

Two phase flow is a flow pattern where either the fluid flows through two different regions (non-porous or porous region) or two different fluids (with different viscosities). In this

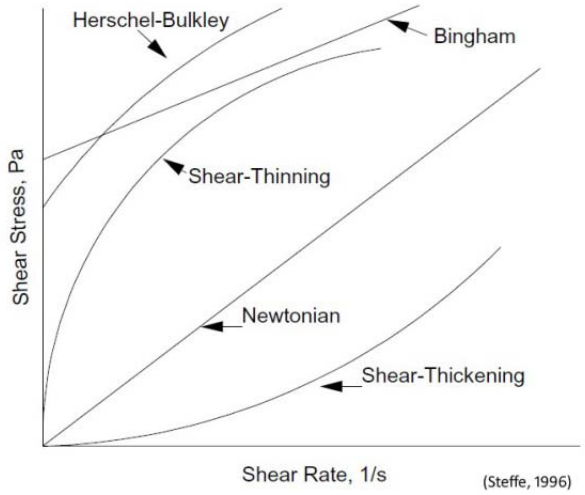

Figure 1.3: Qualitative flow curves for different types of time-independent fluids, (www.engineeringarchives.com)

study the Newtonian fluid and Non-Newtonian fluid model were combined and the flow was divided into two-phases. Blood flow in microvessels demonstrates a two-phase flow with a peripheral layer of plasma showing a Newtonian nature and a core region of vessels showing a non-Newtonian nature.A non-Newtonian region can be represented by Casson model/Herschel-Bulkley model/Power law model/Bingham model.

Chapter 2

The impact of stress jump condition and heterogeneous reaction on velocity and concentration during bio-fluid flow through a permeable microvessel

---

2.1 Introduction

The study of fluid dynamics of basic biological fluids such as blood has been considered as a great tool of biomedical engineering in recognizing the cause of certain diseases and making it easy to come up with ways to cure the diseases (Mazumdar [16]). Blood is a complex body (liquid tissue) consisting of several types of formed elements (cells) suspended in an aqueous fluid matrix (plasma). Blood flows in different ways depending on the channel it is flowing in. The flow can be in a closed circulating system (veins, arteries and capillaries) or an open circulatory system (heart etc). Nanda and Basu Mallik [25] pointed out that blood behaves like a homogeneous Newtonian fluid in large blood vessels while in narrow blood vessels it behaves like a non-Newtonian fluid.

The study of heat transfer in a living tissue is an interesting concept and many mathematical models have been formulated for the purpose of studying thermal regulation or other

phenomena where significant heat exchanges have taken place (Chen and Holmes [5]). The bio-heat equation during blood flow through vessel has been expressed by Pennes [27] based on his experimental outcomes. An analytical solution of the Pennes equation on bioheat has been studied by Huang et al. [14] and Yue et al. [51].A porous medium (aperipheral layer for the microvessel) plays a vital role in the heat transfer process in blood vessel (Khaled and Vafai [15]). Sinha et al. [38] highlighted the heat transfer for a unsteady blood flow in a permeable vessel. They have introduced non-uniform heat source. The effect of magnetic field on the heat transfer of two-phase blood flow through a stenosed artery has been discussed by Ponalagusamy and Selvi [28]. The governing parameters that influence heat transfer and corresponding mathematical models are discussed at length by Fasano and Sequeira [10].

Solutal transport along with heat transfer are responsible for different activities such as secretion of insulin, gastric acid etc, It is more prompted during drug delivery (Sushma et al. [47]). The impact of both thermal diffusion and solutal reaction on blood flow plays a vital role in the concentration difference and rate of change in heat transfer (Xu et al. [49]). Heat and mass transfer for a physiological fluid has been studied by Misra and Adhikary [17]. Das and Chakraborty [6] studied the electroviscous effect on the velocity, temperature and concentration distribution of a non-Newtonian biofluid.

The purpose of this chapter is to study blood flow velocity, temperature and dispersion through a permeable microvessel with stress jump condition and velocity slip condition. Considering a two phase non-Newtonian fluid model, where the radius of the microvessel is divided into two parts with clear region and peripheral layer of plasma. A clear region is defined to be a non-Newtonian Casson fluid with blood cells, mainly Red blood cells, while a peripheral layer of plasma is defined to be a Newtonian fluid. The concentration profile is divided into two-phases, in the same manner as the velocity profile. However, the temperature profile is considered as a single phase. The governing equations for velocity, temperature and concentration are solved analytically and the results established through graphs.

2.2 Mathematical Formulations

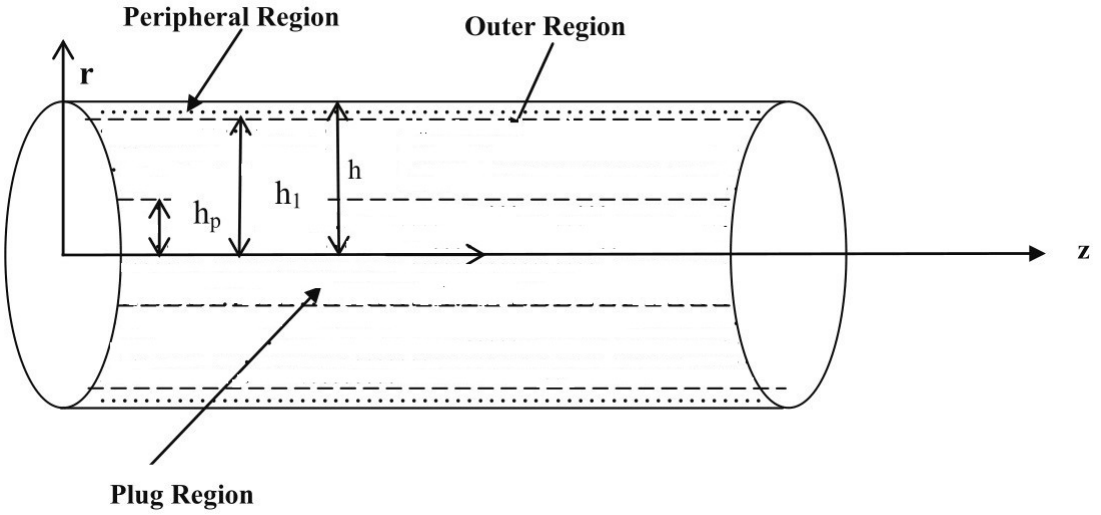

Figure 2.1: schematic diagram of the two-phase non-Newtonian Casoon model of two-phase blood flow in a permeable microvessel

Since blood vessels are kind of circular, a cylindrical polar coordinate system (r, θ, z) is considered where the z-axis is along the axis of the microvessel, and r and θ are coordinates along the radial and circumferential directions respectively. The flow along the microvessel is described by a two phase non-Newtonian Casson model and the wall of the microvessel is assumed to be permeable following the Brinkman Model nature, with slip condition at the wall. A clear region is taken to be a non-Newtonian Casson fluid which is of radius h_2. The radius of the plug region is h_1, $h - h_2$ being the thickness of the peripheral region taken to be a Newtonian fluid as shown in Fig. 2.1. It is assumed that the flow is fully developed and axi-symetric.

2.2.1 Velocity Profile

The governing equations for the two-phase Casson fluid with the Brinkman model at the peripheral region may be written as follows

$$\frac{\partial U_p}{\partial r} = 0, \ 0 \leq r \leq h_1, \tag{2.1}$$

$$\frac{\partial p}{\partial z} = \frac{-1}{r}\frac{\partial}{\partial r}\left[r\left(\tau_y^{1/2} + \left(-\mu_1 \frac{\partial U_1}{\partial r}\right)^{1/2}\right)^2\right], \quad h_1 \leq r \leq h_2, \tag{2.2}$$

$$\frac{\partial p}{\partial z} = \frac{\mu_2}{r}\frac{\partial}{\partial r}\left(r\frac{\partial U_2}{\partial r}\right) - kU_2, h_2 \leq r \leq h, \tag{2.3}$$

where p is the pressure, U_p, U_1 and U_2 are axial velocities in the plug region, core region and peripheral region respectively. And τ_y is the yield stress, μ_1 and μ_2 are viscosities of the fluid in the core region and peripheral region, respectively.

Associated boundary conditions are

$$\frac{\partial U_p}{\partial r} = 0, \text{ at } r = 0, \tag{2.4}$$

$$U_p = U_1, \text{ at } r = h_1, \tag{2.5}$$

$$U_1 = U_2 \text{ and } \frac{\partial U_1}{dr} = \mu_2 \left(\frac{\partial U_2}{\partial r} - \beta U_2 \right) \text{ at } r = h_2, \tag{2.6}$$

$$\frac{\partial U_2}{\partial r} + \gamma U_2 = 0, \text{ at } r = h. \tag{2.7}$$

Solving the above governing equation analytically (as it is show in the appendix) and using the associated boundary condition we get the velocities as follows

$$U_p = \frac{h_1^2}{4\mu_1}\frac{\partial p}{\partial z} - \frac{h_1 \tau_y}{\mu_1} + \frac{4h_1^{3/2}}{3\mu_1}\sqrt{\frac{-\tau_y}{2}\frac{\partial p}{\partial z}} + B, \tag{2.8}$$

$$U_1 = \frac{r^2}{4\mu_1}\frac{\partial p}{\partial z} - \frac{r \tau_y}{\mu_1} + \frac{4r^{3/2}}{3\mu_1}\sqrt{\frac{-\tau_y}{2}\frac{\partial p}{\partial z}} + B, \tag{2.9}$$

$$U_2 = m_1 J_0(\lambda r) + m_2 Y_0(\lambda r) + \frac{\kappa}{\lambda^2}, \tag{2.10}$$

where $\lambda^2 = \frac{-k}{\mu_2}$, $\kappa = \frac{1}{\mu_2}\frac{dp}{dz}$, m_1, m_2 and B is found in the appendix.

Volumetric flow rate is

$$Q = 2\pi \int_0^h r u dr, \tag{2.11}$$

expressed as

$$Q = 2\pi \left[\int_0^{h_1} r U_p dr + \int_{h_1}^{h_2} r U_1 dr + \int_{h_2}^{h} U_2 dr \right], \tag{2.12}$$

Thus the average velocity of blood flow through the microvessel is

$$\cup = \frac{Q}{\pi h^2}. \tag{2.13}$$

2.2.2 Temperature

Using the concept of the Pennes' equation (Pennes [27], Yue et al. [51]), the one dimensional bioheat equation for the steady state and the absence of external spatial heating can be written as follows

$$\frac{\partial}{\partial r}\left(r\frac{\partial T}{\partial r}\right)+\frac{q_m}{K_b}=\frac{W_bC_b}{K_b}(T-T_A), \tag{2.14}$$

where T is the temperature which is a function of r, q_m is the metabolic heat generation per unit volume, W_b is the perfusion rate of blood, C_b is the specific heat of the blood, K_b is the thermal conductivity of the surrounding tissue of the blood vessel and T_A is the arterial temperature. Using the method of undetermined coefficient to solve the governing equation using the boundary conditions below

$$\frac{\partial T}{\partial r}=0 \ at \ r=0, \tag{2.15}$$

$$T=T_w \ at \ r=h, \tag{2.16}$$

where T_w is the wall temperature due to the surrounding tissue of the blood vessel. We get

$$T=L_1J_0(r\sqrt{-G})+L_2Y_0(r\sqrt{-G})+T_A+\frac{q_m}{w_bC_b}, \tag{2.17}$$

with $G=W_bC_b/K_b$. Since Temperature is finite at $r=0$,we have L_2 is zero, Hence

$$T=L_1J_0(r\sqrt{-G})+T_A+\frac{q_m}{w_bC_b}, \tag{2.18}$$

where $L_1=\frac{T_w-T_A}{J_0(h\sqrt{-G})}$.

2.2.3 Concentration Profile

Following the approach proposed by Taylor [48], a cylindrical frame of reference (r,z), like the one in Fig. 2.1. The governing advection-Diffusion equation is given by

$$\frac{U(r)}{Dm}\frac{\partial C}{\partial z}+\frac{1}{Dm}\frac{\partial C}{\partial t}=\frac{1}{r}\frac{\partial}{\partial r}\left(r\frac{\partial C}{\partial r}\right)+\frac{\partial^2 C}{\partial z^2}, \tag{2.19}$$

where u(r) is non-uniform axial velocity, C(r,z,t) is solute concentration and Dm is the Diffusion coefficient. With the aid of Taylor's approximation, the governing equation can be reduced (Taylor, [48]), and the reduced equation

$$\frac{1}{r}\frac{d}{dr}\left(r\frac{dC}{dr}\right)=\frac{\hat{U}(r)}{Dm}\frac{dC}{dz}, \tag{2.20}$$

where $\hat{U}(r)=U(r)-\cup$ is the velocity deviation from the mean $\cup$ (Das et al, [6]).

Solving the reduced equation (2.20) using the same approach used to get equation (2.8)-(2.10) the plug, core and peripheral region velocities are used together with the following boundary conditions

$$C = \frac{\partial C}{\partial r} = 0 \quad \text{at } r = 0, \tag{2.21}$$

$$C_1 = C_p \quad at\ r = h_1, \tag{2.22}$$

$$C_1 = C_2, \qquad \frac{\partial C_1}{\partial r} = \frac{\partial C_2}{\partial r} \quad \text{at } r = h_2, \tag{2.23}$$

$$\frac{\partial C_2}{\partial r} + \gamma C_2 = -\frac{1}{D_m}\frac{\partial C}{\partial z} \text{ at } r = h, \tag{2.24}$$

we get

$$C_p = \frac{U_p}{D_m}\frac{\partial C}{\partial z}\frac{r^2}{4}, \tag{2.25}$$

$$C_1 = \left(\frac{r^4}{64\mu_1}\frac{\partial p}{\partial z} - \frac{r^3}{9}\frac{\tau_y}{\mu_1} + \frac{16}{147}\frac{r^{\frac{7}{2}}}{\mu_1}\sqrt{\frac{-\tau_y}{2}\frac{\partial p}{\partial z}} + \frac{Br^2}{4}\right)\frac{1}{D_m}\frac{\partial C}{\partial z} + B_1 lnr + B_2, \tag{2.26}$$

$$C_2 = \left(\frac{m_1}{\lambda^2}J_0(\lambda r) - \frac{m_2}{\lambda^2}Y_0(\lambda r) + \frac{r^2}{4}\frac{\kappa}{\lambda^2}\right)\frac{1}{D_m}\frac{\partial C}{\partial z} + B_3 lnr + B_4, \tag{2.27}$$

where $B_1, B_2, B_3 \text{and} B_4$ are found in the appendix.

2.3 Results and Discussion

The governing equations for velocity, temperature and solute concentration of blood flow in permeable microvessel are solved analytically with the help of boundary conditions and written in the form of general and modified Bessel functions. Subsequently, these profiles were plotted against radius. For some fixed parameters $\beta = 0.1, \gamma = 0.02, \tau_y = 0.15, \frac{dp}{dz} = 10$ and $k = 1$. The impact of different parameters such as stress jump constant, slip constant, yield stress, pressure gradient and permeability constant are shown through Fig. 2.2 - 2.16.

The blood flow through a microvessel is complicated in the present of red blood cells which creates an additional region closer to the axis. Due to rotation nature, RBCs are accumulated closer to the axis of the microvessel and behave as a semi-solid cylinder of radius h_p, width of the plug region. The velocity of this region is constant or rather it has a zero velocity gradient. The width of the plug region is taken as 0.3 and hence the constant velocity profile will be continued till $r = 0.3$. However, a significant change has

been noticeable at $r = 0.9$, which is the interface of the clear region and peripheral region. A similar profile of the velocity is observed for all cases.

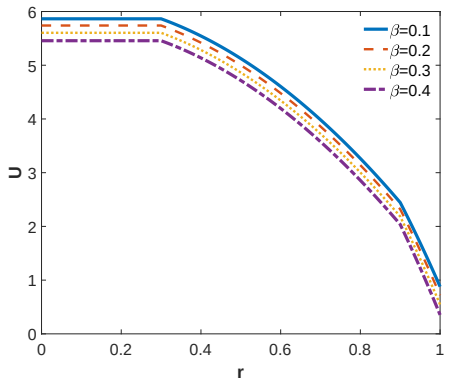

Figure 2.2: Velocity radius graph with different stress jump constant β

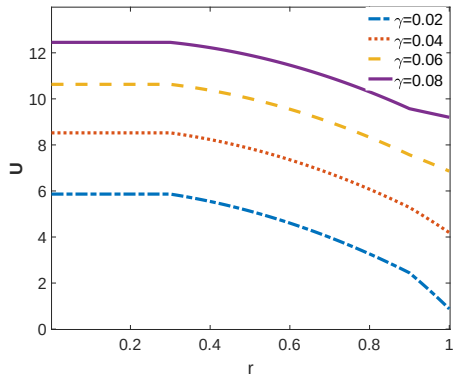

Figure 2.3: Velocity radius graph with different slip constant γ

Stress jump condition is taken place at the interface of the fluid region and peripheral region which in this case is a porous medium. It represents a jump of stress between two regions. It is evident that with increase in the stress jump condition, the stress difference between two region is increasing and it introduces an additional stress which may cause for the reduction in velocity profile as shown in Fig. 2.2.

The slip condition at the interface of the microvessel taken place due to permeability nature of the inner wall of the microvessel. It gives a non-zero velocity at the inner surface. The nature of the velocity is more significant near the wall, at the peripheral region. From Fig. 2.3, it is observed that for a higher value of slip constant (γ), the slope of the velocity is going upwards at the peripheral region and it reduces the velocity difference. The stiffness is more for a higher slip constant ($\gamma = 0.5$) and almost slit for $\gamma = 0.02$.

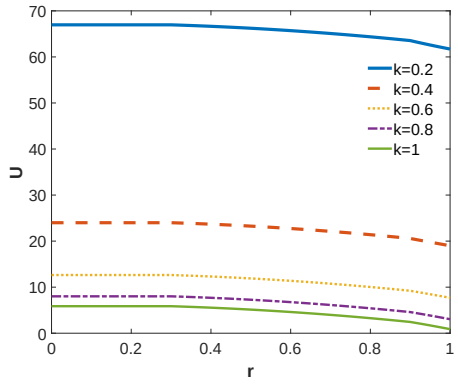

Figure 2.4: Velocity radius graph with different permeability constant K

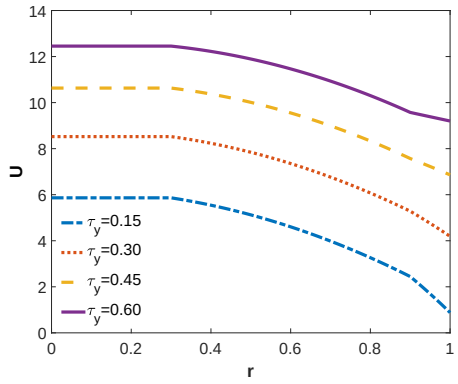

Figure 2.5: Velocity radius graph with different yield stress τ_y

The permeability related with the porous medium which is containing the pores and fluid passes through those pores which triggers a restriction on the flow. Hence the flow is not faster than the clear region, as a result the fluid velocity decreases with an increase of the permeability parameter as shown in Fig. 2.4.

Another very important parameter which appears due to the Casson fluid nature of the blood at the clear region is yield stress; it is directly proportional to the pressure gradient. It should be noted that with an increase in yield stress, the velocity of the fluid increases but the slope become more stiff for the higher value of yield stress as one would observe in Fig. 2.5.

Displayed in Fig. 2.6 the influence of the pressure gradient on the velocity profile. Evidently, the velocity of the fluid is higher closer to the axis as increase in the pressure gradient. The velocities for different pressure gradients coincide at one point, which is $r = 0.65$ in this case. It is interesting to note that the stiffness of the velocity is higher for a higher value of the pressure gradient.

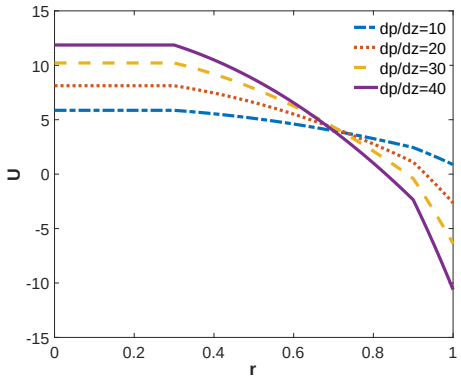

Figure 2.6: Velocity radius graph with different pressure gradient parameters

The concentration profile followed a zero concentration at the plug region. After that there is an improvement in the concentration with radial direction. This profile is followed in all the cases. The concentration of the solute is decreasing with an increase in the stress jump condition, this is because of the decreasing in velocity which again retained the solute concentration (see Fig. 2.7). From Fig. 2.8, it is evident that the slip constant at the surface of the microvessel increases the concentration of the solute. The profile of the concentration is the same as the previous. For the values of the slip constant we considered $0.02, 0.04, 0.06$ and 0.08 and it is evident that the concentration difference is higher between the lower values of the slip constant i.e. between $\gamma = 0.02$ and 0.04. The concentration of the solute is a decreasing function of the permeability parameter as same as the velocity (see Fig. 2.9). Again the difference of the two consecutive concentration is higher for the difference between two consecutive lower permeability parameter.

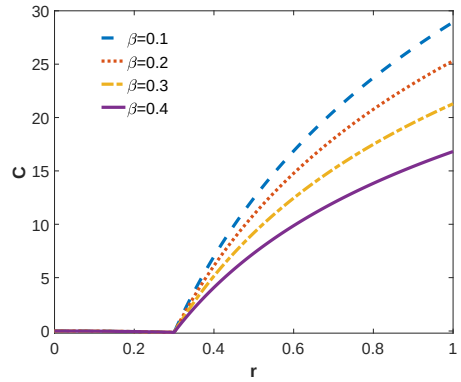

Figure 2.7: Velocity radius graph with different stress jump constant β

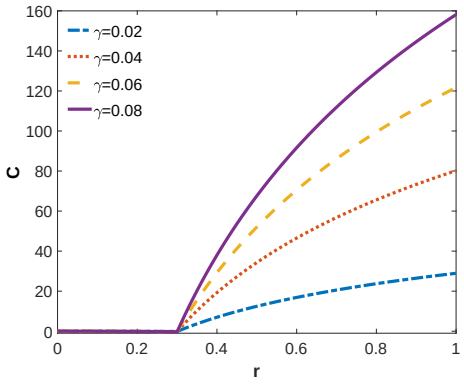

Figure 2.8: Concentration radius graph with different slip constant γ

The yield stress which is related to the nature of the Casson fluid acts mainly at the clear region, enhances the concentration profile through the radius of the microvessel. However, an opposite phenomena is observed when comparing the difference of the two consecutive concentrations, which is higher in this case for the difference between two consecutive higher yield stress, as visible in Fig. 2.10. Initially, the pressure gradient enhanced the concentration of the solute but for higher values it shows a stable concentration profile. Figure 2.11, shows proof that the concentration profile did not significantly change for $dp/dz = 30$ and $dp/dz = 40$.

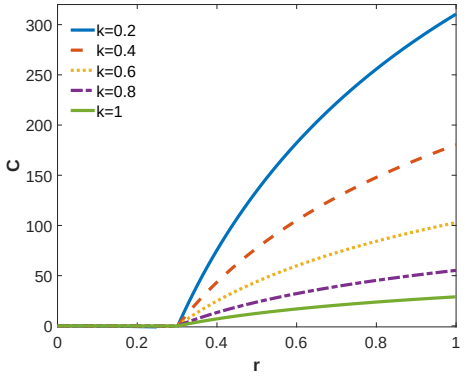

Figure 2.9: Concentration radius graph with different permeability constant K

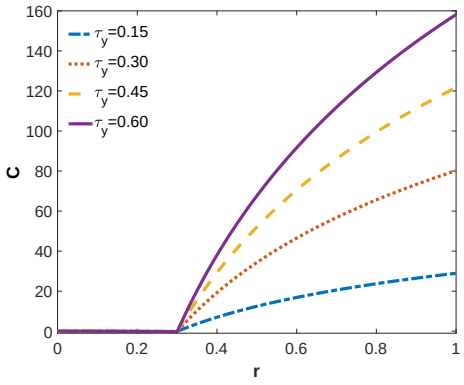

Figure 2.10: Concentration radius graph with different yield stress τ_y

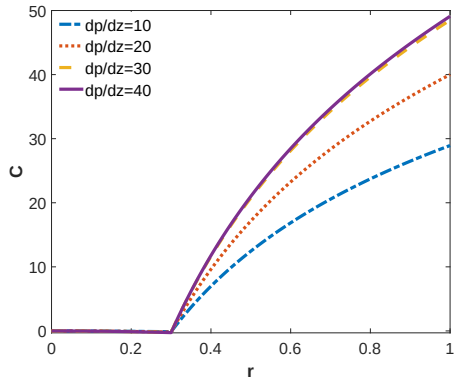

Figure 2.11: Concentration radius graph with different pressure gradient

The temperature profile bears a noteworthy difference. The temperature of the blood (T_A) and temperature at the inner surface of the microvessel which is basically due to the temperature of the surrounding tissue, are considered different in values. Despite the preceding, the temperature at the surface of the inner wall is considered higher than the temperature of the blood. The motion of the RBCs is constant near the axis and they are unable to distribute the temperature through out. As a result, the temperature decreases significantly at the plug region and it continue at the outer region which is basically a cell depleted region (absence of RBCs). Due to the cell depleted nature the temperature reduction continues until $r = 0.65$. Afterwards, there is an increment in the temperature profile, this goes on until the surface of the wall. This enhancement is related to the temperature of the inner surface which is higher than the temperature of the blood, for this reason it influences the heat transfer towards the axis and increasse the temperature closer to the surface. This general phenomena is observed for all the cases. The nature of the temperature profile for different values of the stress jump constant is the same as the

velocity and concentration profile, that is the temperature profile is increasing with every increase in the stress jump constant (see Fig. 2.12). Notably, the temperature near the axis is higher than the temperature at the surface except when $\beta = 0.1$.

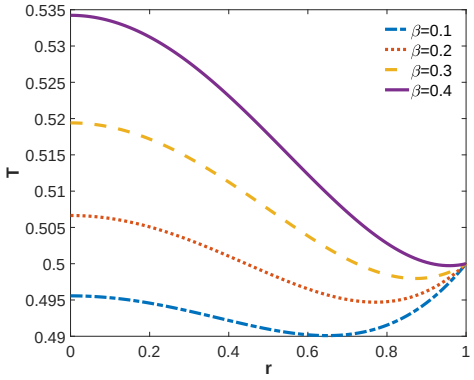

Figure 2.12: Temperature radius graph with different stress jump constant β

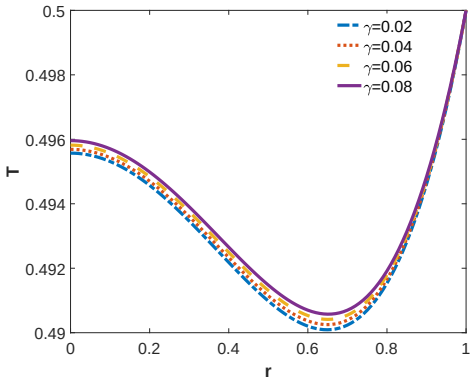

Figure 2.13: Temperature radius graph with different slip constant γ

The temperature profile curve is more captivating and significant with respect to the slip velocity condition at the inner surface of the wall. Initially, the temperature gradient is negative, while after $r = 0.65$ the gradient becomes positive. It observed that the stiffness of the positive gradient is higher that the stiffness of the negative gradient (see Fig. 2.13). The temperature profile is increasing with an increase in the slip constant but the difference is not significant.Clearly the temperature distribution is much higher at the clear region than the peripheral region as reflected in Fig. 2.14. In all the cases, the temperature at the axis is higher than the temperature at the surface of the microvessel.The temperature profile is constant with respect to radial direction for $K = 1$ and it carried a constant value 0.5.

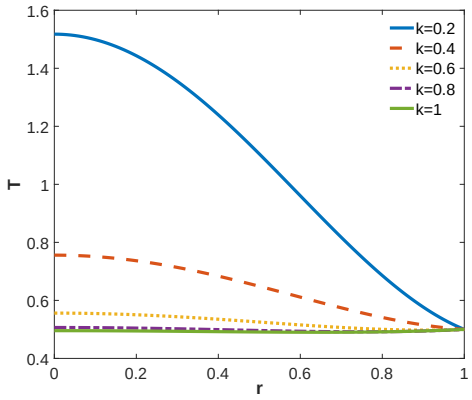

Figure 2.14: Temperature radius graph with different permeability constant K

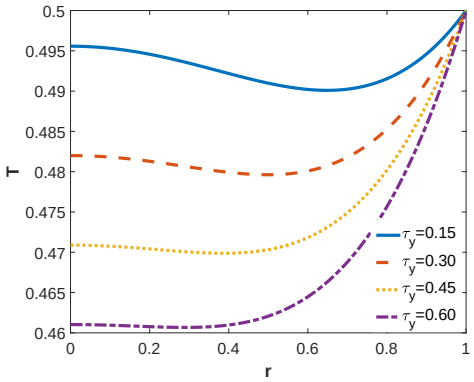

Figure 2.15: Temperature radius graph with different yield stress τ_y

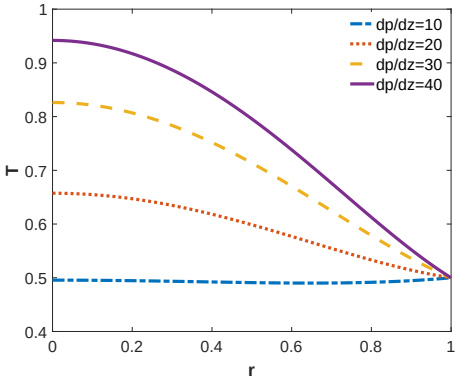

Figure 2.16: Temperature radius graph with different pressure gradient

Interestingly, the temperature at the axis is always lower than the temperature at the surface of the microvessel under consideration of the yield stress values of $0.15, 0.30, 0.45$ and 0.60 (see Fig. 2.15). The temperature at the axis is decreasing with increase in the yield stress. As pressure gradient increases, it enhances the velocity of the solute which

is equally responsible for the distribution of temperature. And it is very natural that the pressure gradient enhances the temperature at the axis and through out the radial direction. At the axis the temperature is higher than the temperature at the surface for most of the cases ($dp/dz = 20, 30, 40$) while it is lower for the lower pressure gradient. As a result, we get two different patterns of the temperature profile for larger and smaller values of the pressure gradient as displayed in Fig. 2.16. In the case of a lower pressure gradient (here $dp/dz = 10$), the temperature profile is not significant but it slightly increases with radial direction.

2.4 Conclusion

This chapter explores the velocity, temperature and concentration of blood flow through a permeable microvessel. The velocity and concentration profile are divided into three regions that is, the plug region, the outer region and the peripheral region. The influence of the stress jump condition, the slip condition of velocity and concentration , the yield stress, the pressure gradient and the permeability of the peripheral region plays an important role which is well reflected through graphs. In general it is observed that the velocity and concentration at the plug region is constant while after this the velocity decreases through out the radius. However the concentration increases continuously in the radial direction. Velocity is non-zero at the walls of the microvessel because of the slip constant γ and the stress jump constant causes a rapid decrease in velocity between the core region and the peripheral region. The temperature profile is showing two different trends that is high temperature at the wall of the microvessel with low temperature at the axis and low temperature at the wall of the microvessel with high temperature at the axis. This works gives an overall idea of blood flow in sense of velocity, temperature and concentration under certain condition.

Chapter 3

Steady Solute dispersion in Herschel-Bulkley fluid in a permeable microvessel

3.1 Introduction

The dispersion of solutes has been a great topic due to its wide application in fields such as medical engineering, chemical engineering, environmental engineering etc. A large number of scientiests and engineers have dedicated their lives to the study of solute dispersion in different environments, circulatory systems being one of them. Theory of solute dispersion was first introduced by Taylor [48] around 1950's, Taylor analytically and experimentally studied solute dispersion in a steady laminar viscous fluid flow via a straight tube, later Aris [1] developed Taylor's concept using the method of moments, taking into consideration the axial diffusion term which was neglected by Taylor [48]. Since these studies were mainly based on the study of solute dispersion at large times but not at small times after injection of solutes in the fluid, Gill and Sankarasubramanian [13] proposed a generalized dispersion model of solute dispersion, which is now widely used together with Taylor-Aris dispersion theory by many reseachers in the study of solutes dispersion. Furthermore Sharp [41] following Taylor approach [48] studied shear-augmented dispersion in non-Newtonian fluids and showed that the dispersion of solutes depends on specific rheological parameter of the fluid that is yield stress. Decuzzi et al. [7], Gentile et al. [12] also revisited

Taylor and Aris theory studying longitudinal diffusion.Different models are used to study solute dispersion depending on the environment e.g in the cardio-vascular system blood flows in different ways, depending on the channel it is flowing in, it can either be in closed circulatory system(veins,ateries and capillaries) or an open circulatory system(heart). In large blood vessels blood behaves like homogeneus Newtonian fluid and behaves like a non Newtonian fluid in narrow blood vessels (Mazumdar [16]). Blood flow presents a remarkable two-phase nature, when it flows via small vessels or channels, there will be a peripheral layer of plasma (Newtonian fluid) and a core region of erythrocytes (non-Newtonian fluid), all this was proved by Bugliarell and Sevilla [4].

Of late both unsteady and steady solute dispersion have been getting more attention both in science and engineering research. Rana and Murthy [35] studied unsteady solute dispersion in small blood vessels using a two phase Casson model. Gentile et al. [12] studied the transport of nanoparticles in blood vessels; The effect of vessel permeability and blood rheology using Casson fluid law. Shaw et al. [45] studied magnetic drug targeting in permeable microvessel using a two-phase Casson model and later used the same model to study dispersion characteristics of blood during nanoparticle assisted drug delivery process through a permeable microvessel, ignoring time factor (Shaw et al, [42]). In many cases, researchers use a two-phase casson model to study blood rheology in microvessels, since it is more realistic and can be manipulated analyticaly. According to the author's knowledge, very few researchers have used a two-phase Herschel-Bulkely model. Using a two phase Herschel-bulkely model, Nallapu and Radhakrishmacharga [18] derived analytical solutions for velocity, flow flux, effective viscosity, core hematocrit and mean heamatocrit. Since blood is closely decribed as Herschel-Bulkley fluid in narrow tubes (Nallapu et al, [18]), in this study we consider the same.

The purpose of this chapter is to study the significance of the nature of microvessel walls and rheology of blood on the dispersion of solutes. We consider a two phase Herschel-Bulkely flow, where the microvessel is divided into peripheral region and and core region which includes the plug region. Blood in the peripheral region obeys the Newtonian fluid character and in the core region blood obeys the non-Newtonian Herschel-Bulkely fluid character. The Darcy model is used to characterize the permeable nature of the microvessel's inner wall. The effect of blood rheological parameter, permeability parameter, pressure constant, particle volume fraction, stress jump constant, slip constant and yield stress on the dispersion of the particles are reflected on the study. The results of this study is important since it brings a better understanding of the effect of all rheological

parameters and providing new insights in biomedical engineering.

3.2 Mathematical formulation

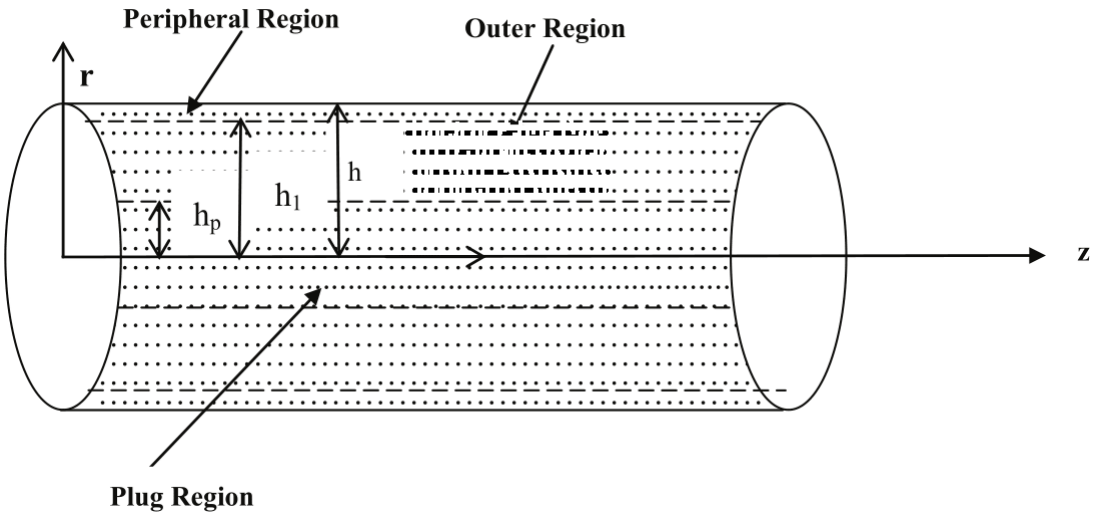

Figure 3.1: schematic diagram of two-phase blood flow in a permeable microvessel

Since blood vessels are primarily of circular geometry, we consider a cylindrical polar coordinate system (r, θ, z) where the z-axis is along the the axis of the microvessel, r and θ are coordinates in the radial and circumferential directions, respectively. The flow along the microvessel with radius h is considered as two-phase in nature, the core region (non-peripheral) is taken to be a non-Newtonian Herschel-Bulkely fluid which is of radius h_1 with $h - h_1$ being the thickness of the peripheral region taken to be a Newtonian fluid as shown in Fig. 3.1. The following assumptions are made: (a) the flow is fully developed and axi-symetric, (b) the wall of the microvessel is permeable and a Darcy model is used to define the permeability of the wall, (c) the fluid flows laterally across the vessel fenestration.

3.2.1 Modelling of apparent viscosity

Viscosity differs in different environments. According to Fahraeus and Lindqvist [9] the viscosity of a fluid is directly proportional to the diameter of the tube, and this is true for blood flowing inside a microvessel, because erythrocytes migrate to the center of the vessel, leaving only plasma near the wall of the vessel. Pries and Secomb [29] experimentally

determined te blood viscosity in the core region(μ_{core}) of a microvessel as

$$\mu_{core} = \mu_{plasma}\left[1 + (\mu_{0.45} - 1)\frac{(1-H_D)^{CC} - 1}{(1-0.45)^{CC} - 1}(\frac{d_v}{d_v - 1.1})^2\right]\left(\frac{d_v}{d_v - 1.1}\right)^2, \tag{3.1}$$

where $\mu_{plasma} = 0.0012Ns/m^2$ is the viscosity of the blood plasma without cells and platelets, d_v is the diameter of the blood vessel in a micron, H_D is the haematocrit ranging between $0.39 - 0.45$, $\mu_{0.45} = 6e^{-0.085d_v} + 3.2 - 2.44e^{-0.06d_v^{0.645}}$, $CC = (0.8 + e^{-0.075d_v})\left(\frac{1}{1+10^{-11}d_v^{12}} - 1\right) + \frac{1}{1+10^{-11}d_v^{12}}$.

A few models have been developed theoretically to explain the viscosity of the particle suspension. Einstein [8] predicted the effective viscosity (μ_{eff}) of suspension as

$$\mu_{eff} = \mu_{bf}(1 + 2.5\phi), \tag{3.2}$$

where ϕ is the volume fraction of the nanoparticle and μ_{bf} is the base fluid viscosity. Later Brinkman [3] generalized this model, since it is only valid for a low volume fraction of approximately 0.02. According to Brinkman [3] the effective viscosity of the nanofluid can be written as

$$\mu_{nf} = \mu_{bf}(1 - \phi)^{-2.5}. \tag{3.3}$$

Later Pasol and Feuillebois [26] gives the viscosity of the nanofluid μ_{nf} as,

$$\mu_{nf} = \mu_{bf}\left(1 + 2.5\left[1 - 3.4606\frac{d_p}{d_v} + 8.6065(\frac{d_p}{d_v})^2\right]\phi\right), \tag{3.4}$$

where d_p is the diameter of the suspended particle. According to Shaw et al. [42] the viscosity of the blood is influenced by the nanoparticle suspensions and the diameter of a microvessel. Hence the viscosities of the blood with nanoparticles at the core region, μ_1, and the peripheral region, μ_2, respectively can be taken as

$$\mu_1 = \mu_{core}\left(1 + 2.5\left[1 - 3.4606\frac{d_p}{d_v} + 8.6065\left(\frac{d_p}{d_v}\right)^2\right]\phi\right), \tag{3.5}$$

$$\mu_2 = \mu_{plasma}\left(1 + 2.5\left[1 - 3.4606\frac{d_p}{d_v} + 8.6065\left(\frac{d_p}{d_v}\right)^2\right]\phi\right). \tag{3.6}$$

3.2.2 Velocity of the fluid

The mass continuity equation can be written as

$$\frac{\partial \dot{Q}}{\partial z} + v_p\lambda_p = 0, \tag{3.7}$$

$\dot{Q}$ being the flow rate, λ_p being the perimeter of the permeable microvessel, $v_p\lambda_p$ he volume rate along the permeable wall per unit length, and v_p the perfusing velocity derived from Darcy's law, written as

$$v_p = -L_p(\pi_i - p), \tag{3.8}$$

where $L_p = \frac{k}{\eta\delta}$ is the hydraulic conductivity, δ is the thickness of the microvessel wall, k is the permeability of the microvessel wall and η is the effective viscosity of the fluid. Interstitial fluidic pressure is denoted by π_i and p is for the local mean value of the vascular pressure. p_0 and p_1 are inlet and outlet vascular pressures, respectively.

To calculate the flow rate, we first calculate the axial velocity using the following equations

$$\frac{\partial u_p}{\partial r} = 0, \quad 0 \le r \le h_p, \tag{3.9}$$

$$\frac{\partial p}{\partial z} = -\frac{1}{r}\frac{\partial}{\partial r}\left[r\left(\tau_y + \left(-\mu_1\frac{\partial u_1}{\partial r}\right)^n\right)\right], \quad h_p \le r \le h_1, \tag{3.10}$$

$$\frac{\partial p}{\partial z} = -\frac{\mu_2}{r}\frac{\partial}{\partial r}\left(r\frac{\partial u_2}{\partial r}\right), \qquad h_1 \le r \le h, \tag{3.11}$$

with the following boundary conditions

$$\begin{aligned} \frac{\partial u_1}{\partial r} = 0, \quad \text{and} \quad u_p = u_1, \quad \text{at} \quad r = h_p, \\ \frac{\partial u_1}{\partial r} = \mu_2\left(\frac{\partial u_2}{\partial r} - \beta u_2\right), \; u_1 = u_2, \quad \text{at} \quad r = h_1, \\ \frac{\partial u_2}{\partial r} + \gamma u_2 = 0, \quad \text{at} \quad r = h, \end{aligned} \tag{3.12}$$

where p is the pressure, u_p, u_1 and u_2 are axial velocities in the plug region, core region and peripheral regions, respectively. τ_y is the yield stress, β the stress jump constant and γ the velocity slip constant.

Solving Eq. (3.9)-(3.11) using boundary condition (Eq. 3.12)(working is in the appendix), the velocity in the plug region, outer region and peripheral region can be written as

$$u_p(r) = B \quad 0 \le r \le h_p, \tag{3.13}$$

$$u_1(r) = \left(\frac{-1}{2\mu_1}\frac{\partial p}{\partial z}\right)^{1/n} \frac{n}{n+1}(r-h_p)^{1+1/n} + K_1 \quad h_p \le r \le h_1, \tag{3.14}$$

$$u_2(r) = \frac{-1}{4\mu_2}\frac{\partial p}{\partial z} r^2 + K_2 \ln r + K_3 \quad h_1 \le r \le h, \tag{3.15}$$

where K_1, K_2 and K_3 are constants provided in the Appendix. Then equations (3.8)-(3.9) are used to calculate the flow rate which is given as

$$\dot{Q} = 2\pi\left[\int_0^{h_p} r u_p dr + \int_{h_p}^{h_1} r u_1 dr + \int_{h_1}^{h} r u_2 dr\right]. \tag{3.16}$$

Hence the corresponding net flow rate is

$$\begin{aligned}\dot{Q} = 2\pi\Bigg[K_1\frac{h_p^2}{2} + \left(\frac{-1}{2\mu_1}\frac{\partial p}{\partial z}\right)^{1/n}\frac{n}{n+1}\left(\frac{nh_1}{2n+1}(h_1-h_p)^{1/n+2} - \frac{n^2}{(2n+1)(3n+1)}(h_1-h_p)^{1/n+3}\right) \\ + \frac{K_2}{2}(h_1^2-h_p^2) - \frac{1}{4\mu_2}\frac{\partial p}{\partial z}(h^4-h_1^4) + \frac{K_2}{2}(h^2\ln h - h_1^2\ln h_1) + (h^2-h_1^2)\left(\frac{K_3}{2}-\frac{K_2}{4}\right)\Bigg]\end{aligned} \tag{3.17}$$

Using Eq. (3.7) and Eq. (3.8) and expressing the flow rate $\dot{Q}$ as a function of the pressure p, we get

$$-\frac{\pi h^4}{8\mu_1}\frac{\partial^2 p}{\partial z}A - L_p[\pi_i - p] = 0, \tag{3.18}$$

where A is a rheological parameter given in the Appendix.

Using the non-dimensional variables $\tilde{z} = z/l_v$,$\tilde{p} = p/\pi_i$, Eq. (3.10) becomes

$$\frac{\partial^2 \tilde{p}}{\partial \tilde{z^2}} + \Gamma^2(\tilde{p}-1) = 0, \ \Gamma = \frac{\prod}{\sqrt{A}} = \frac{4l}{h}\sqrt{\frac{\mu_1 L_p}{\mu_2 h A}}, \tag{3.19}$$

where $\prod$ is the permeability parameter and $\Gamma(A)$ is a constant. Solving Eq. (3.19) using boundary conditions: $\tilde{p}(0) = \tilde{p}_0$, (inlet pressure) and $\tilde{p}(1) = \tilde{p}_1$(outlet pressure), Eq. (3.19) becomes (by ingnoring tilde)

$$p(\Gamma, z) = (p_0 - 1)\cos(\Gamma z) + \frac{(p_1 - (p_0-1)(\cos(\Gamma)-1))}{\sin(\Gamma)}\sin(\Gamma z) + 1. \tag{3.20}$$

Hence the pressure gradient becomes

$$\frac{\partial p}{\partial z} = -\Gamma m_1 \sin(\Gamma z) + \Gamma m_2 \cos(\Gamma z), \tag{3.21}$$

where $m_1 = p_0 - 1, \quad m_2 = \frac{p_1 - (p_0 - 1)(\cos(\Gamma) - 1)}{\sin(\Gamma)}$.

Enabling us to calculate Mean flow velocity ($\cup = \frac{\dot{Q}}{\pi h^2}$) given as

$$\cup = \frac{2}{h^2} K_4 \big[\Gamma m_2 \cos(\Gamma z) - \Gamma m_1 \sin(\Gamma z)\big], \tag{3.22}$$

where K_4 is defined in the appendix.

3.2.3 Effective Longitudinal Dispersion

The transport of solutes within a concentrated suspension of particles can be augmented due to the effects of shear-induced dispersive particle migrations. With the cylindrical coordinate (r,ς,t) system, and the above assumptions, the advection- dispersion equation can be written as Taylor [48]

$$\frac{\partial C}{\partial t} + u(r)\frac{\partial C}{\partial \varsigma} = \frac{D_m}{r}\frac{\partial}{\partial r}\left(r\frac{\partial C}{\partial r}\right) + D_m \frac{\partial^2 C}{\partial \varsigma^2}, \tag{3.23}$$

where C is the solute concentration, $u(r)$ is the axial velocity of the fluid, and D_m is the diffusivity coefficient. Following Taylor (1953), $D_m \frac{\partial^2 C}{\partial \varsigma^2}$ is neglected in Eq. (3.23). Moreover, using the transformation $\varsigma = z - \cup$ with auxiliary frame of reference(r, z) moving with the mean velocity along ς, Eq. (3.23) can be written as follows

$$\hat{u}(r)\frac{\partial C}{\partial z} = \frac{D_m}{r}\frac{\partial}{\partial r}\left(r\frac{\partial C}{\partial r}\right), \tag{3.24}$$

where $\hat{u}(r) = u(r) - \cup$ is the relative velocity about the mean. The following boundary conditions are imposed (Decuzzi et al. [7]; Gentile et al. [12])

$$\begin{aligned} C_p = 0,\ \frac{\partial C_p}{\partial r} = 0, \quad &\text{at } r = 0, \\ C_1 = C_p, \quad &\text{at } r = h_p, \\ C_1 = C_2,\ \frac{\partial C_1}{\partial r} = \frac{\partial C_2}{\partial r}, \quad &\text{at } r = h_1, \\ \frac{\partial C_2}{\partial r} = 0, \quad &\text{at } r = h. \end{aligned} \tag{3.25}$$

Using the above conditions, the same approach for solving equation (3.9)-(3.11) , equation (3.24) gives C_p, C_1, C_2 concentration profile at the plug region ($r < h_p$), core region ($h_p < r < h_1$) and peripheral region ($r > h_1$) as

$$C_p(r) = \frac{\hat{U}_p}{D_m}\frac{\partial C}{\partial z}\frac{r^2}{4}, \tag{3.26}$$

$$\begin{aligned} C_1(r) = \quad & \frac{1}{D_m}\frac{\partial C}{\partial z}\left(\frac{nS_7}{2n+1}\left(\frac{n}{3n+1}\right)(r-h_p)^{1/n+3} - \frac{nS_7}{2n+1}I(r,h_p) + \frac{r^2}{4}\bar{B}\right) \\ & + G\ln r + H, \end{aligned} \tag{3.27}$$

$$C_2(r) = \frac{1}{D_m}\frac{\partial C}{\partial z}\left(\frac{S_8 r^4}{16} + \frac{C}{4}\left(r^2\ln r - r^2\right) + \frac{\bar{D}r^2}{4}\right) + I\ln r + J. \tag{3.28}$$

Following Shaw et al. [42], the flux J of solute across a section at a fixed $\hat{z}$ is given as

$$\begin{aligned} J = \frac{1}{\pi h^2}\Bigg[& \int_0^{h_p} 2r\pi\left(\hat{u}_p C_p - Dm\frac{\partial C}{\partial z}\right)dr + \int_{h_p}^{h_1} 2r\pi\left(\hat{u}_1 C_1 - Dm\frac{\partial C}{\partial z}\right)dr \\ & + \int_{h_1}^{h} 2r\pi\left(\hat{u}_2 C_2 - Dm\frac{\partial C}{\partial z}\right)dr\Bigg], \end{aligned} \tag{3.29}$$

which can be written in a simplified form as

$$\mathrm{J} = \frac{2}{h^2}\left[T_8 + T_9 + T_{10}\right] \tag{3.30}$$

where T_8, T_9 and T_{10} are given in the appendix. The effective dispersion is obtained from the above equation by introducing the Brownian contribution to diffusion

where D_{app} is the apparent dispersion coefficient. The relative effective dispersion is defined as

$$D_{eff} = -\mathrm{J}/\frac{\partial C}{\partial z} = D_m + D_{app} \tag{3.31}$$

The relative effective dispersion (non-dimensional effective dispersion) is defined as

$$D_{eff}/D_m = 1 + D_{app}/D_m \tag{3.32}$$

3.3 Results and Discussion

The influence of the governing parameters such as the pressure parameter Ω, the permeability parameter Π, the nanoparticle volume fraction ϕ, the slip constantγ, the stress jump constant β, the rheology parameter ξ and the yield stress τ_y on relative effective dispersion (equation 3.31) is shown in Figs. (3.2) − (3.8). Four different values of the

power-law index (n) were considered namely, $0.5, 2/3, 1, 3/2$ of the Herschel-Bulkley fluid model ($\tau = \tau_y + k\dot{\gamma}^n$, where τ is the shear stress, $\dot{\gamma}$ the shear rate, τ_y the yield stress,k the consistency index). The value of power-law index expresses the nature of the fluid as shear-thinning or shear-thickening, Mazumdar [16], and with an increase in the power-law index the fluid nature changes from the shear-thinning ($n < 1$) to shear-thickening ($n > 1$) fluid. For $n = 1$, the Herschel-Bulkley fluid reduced to the Bingham plastic fluid. It is important to note that the analytical solution is possible for the above mentioned values of n and for other values of n, therefore we need to go for a numerical solution.

The influence of the non-dimensional pressure distribution on the relative effective dispersion has been discussed in figure 3.2 for different power-law index. The non-dimensional pressure depends on the inlet and outlet pressure which related as $\Omega = (p_0 - 1)/(p_1 - 1)$. In the present chapter, we considered the inlet pressure p_0 as a constant and p_1 as $p_1 = 1 + (p_0 - 1)/\Omega$. It is clear that as Ω decreases (or negative values of Ω increases) the outlet pressure p_1 decreases which leads to a larger difference between the vascular and interstitial pressure and reduces the mean velocity along the microvessel and reflects the same in the dispersion of solutes (Shaw et al [42]). At the same time, the smaller Ω pushes the section with the lower velocity downstream. Consequently, the section with the minimum diffusion moves towards the end of microvessel length which is clearly observed for all the consistency index shown in Fig. 3.2. It is observed that for small values of n, a large value of the flux is archived, and for large values of n, a small value of the flux is archived.

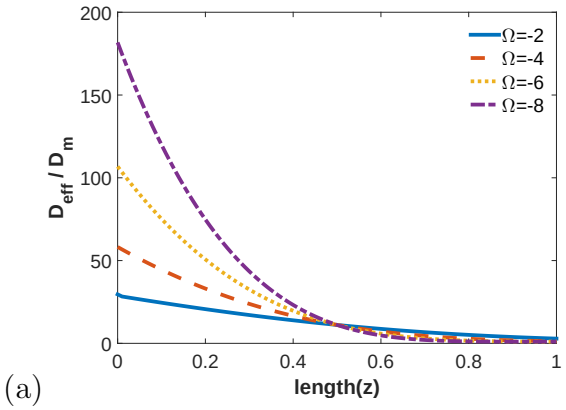

(a)

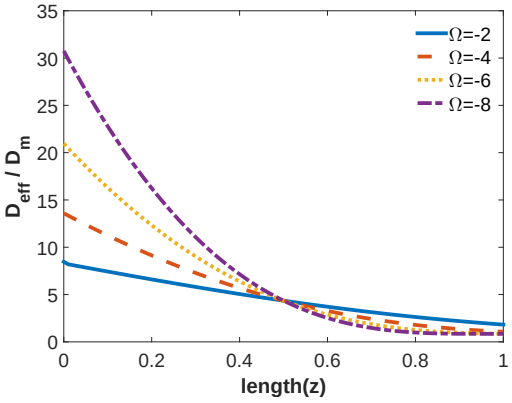

(b)

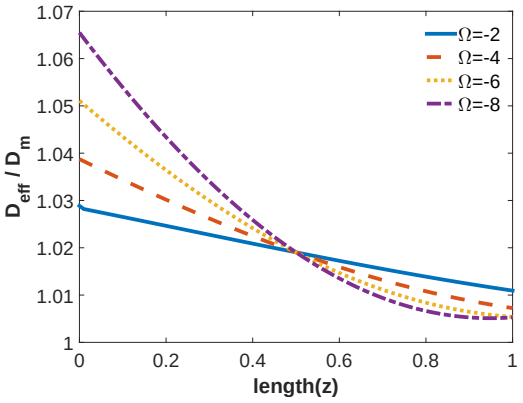

(c)

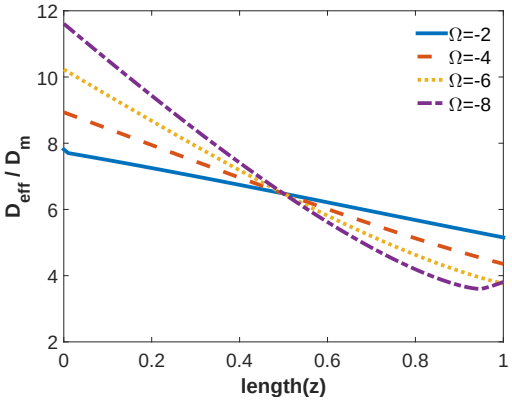

(d)

Figure 3.2: Relative effective dispersion vs axial direction for different pressure parameter when (a) $n = 0.5$, (b) $n = 2/3$, (c) $n = 1$ and (d) $n = 3/2$.

The volume of the nanoparticles plays a vital role in the dispersion characteristics during drug delivery. Nanoarticles are considered spherical with different sizes. In the presence of nanoparticles, nanoparticle-nanoparticle and nanoparticle-RBCs interactions can take place. However, we have neglected both interactions with the exception that they are not occupying the same place (in general RBCs gather near the axis of the microvessel, while the nanoparticles spread towards the wall of the microvessel). As Fullstone et al. [11] mentioned, laminar flow and Brownian motion (for the nanoparticles) influences the motion of the nanoparticles and different phenomena appear at different regions of the microvessel with respect to radius of the microvessel. In the present model, the radius of the microvessel is divided into three regions namely, the plug region, the core region (plasma region) and the peripheral region. Velocity of the blood is higher near to the axis and it vastly decreases near the wall. But, it is non-zero due to the slip condition at the inner surface of the microvessel wall; reducing slowly towards the wall of the vessel. This scenario makes Brownian motion more significant to the displacement of the particle. Therefore, the dispersion has highly taken place closer to the wall. This model, displays relative effective dispersion with respect the the axial direction and it is clear that relative effective dispersion decreases with increases in the volume fraction of the nanoparticles. An increase in the volume fraction of solutes reduces the interparticle distance which disturbs the deformation and rotation of the RBCs, as well as the tumbling of the nanoparticles. The Brownian motion proves more effective for the less volume fraction of the nanoparticles and therefore relative effective dispersion depresses with increase in the volume fraction of nanoparticles as shown in figure 3.3.

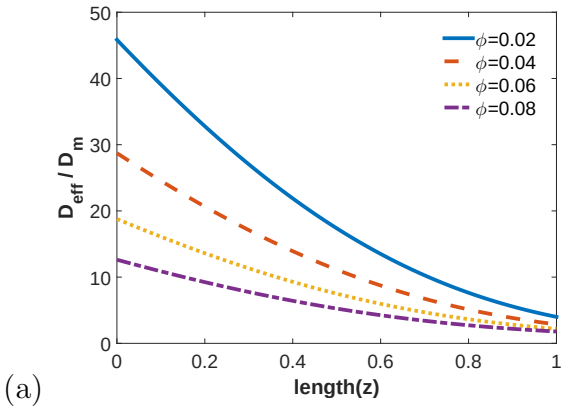

(a)

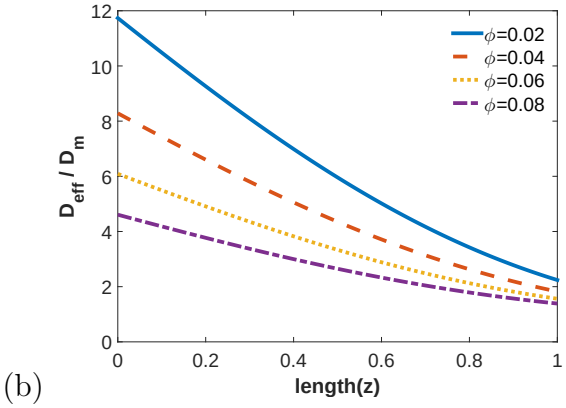

(b)

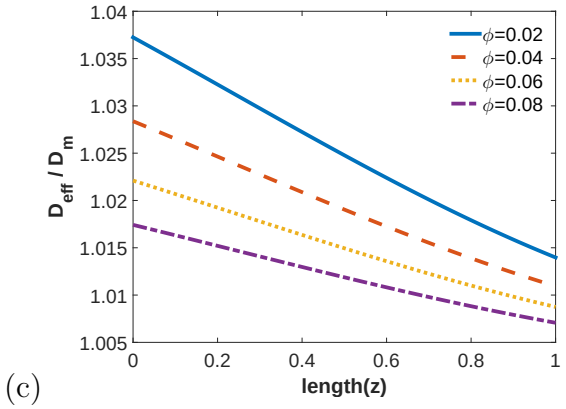

(c)

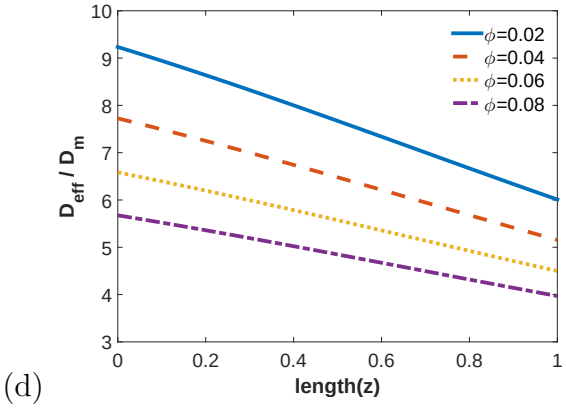

(d)

Figure 3.3: Relative effective dispersion vs axial direction for different nanoparticle volume fraction when (a) $n = 0.5$, (b) $n = 2/3$, (c) $n = 1$ and (d) $n = 3/2$.

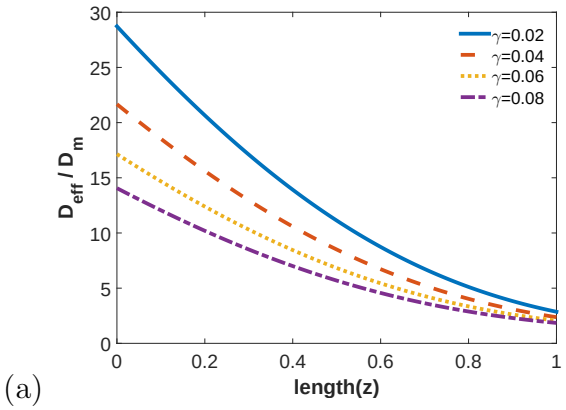

(a)

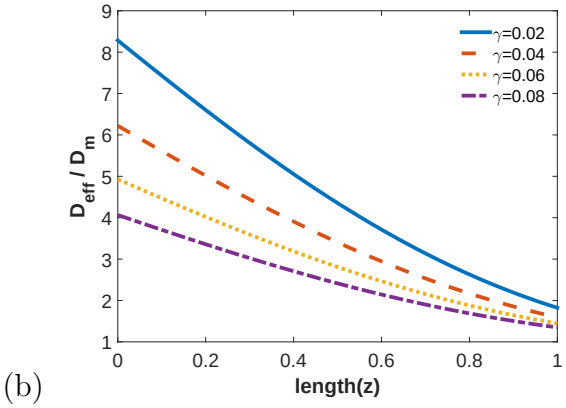

(b)

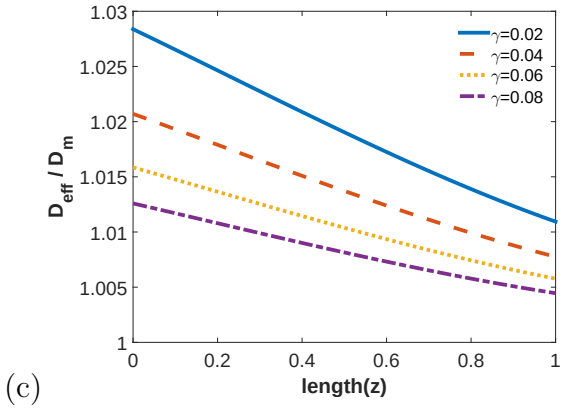

(c)

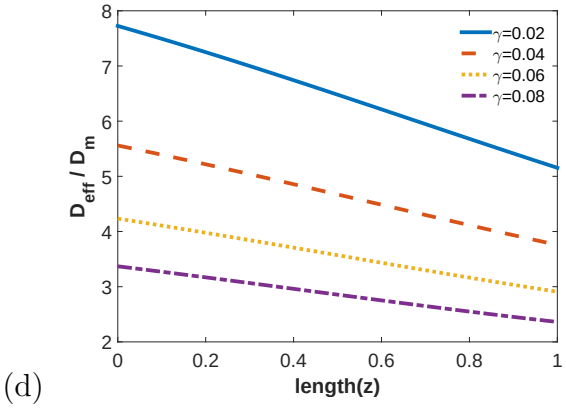

(d)

Figure 3.4: Relative effective dispersion vs axial direction for different slip constant when (a) $n = 0.5$, (b) $n = 2/3$, (c) $n = 1$ and (d) $n = 3/2$.

The present model deals with the slip condition as a consequence of the permeable nature of the inner surface of the microvessel. Due to the slip condition, the velocity at the wall is non-zero and with every increase in the velocity slip condition the velocity gradient at the inner wall of the surface increases and hence the velocity throughout the microvessel. A similar phenomenon is observed by Sinha et al. [39]. With an increase in the axial velocity, the transverse component of the velocity decreases which reduces the dispersion characteristics and a similar impact on relative effective dispersion which is clear from the Figure 3.4. Interestingly under atherosclerosis condition, the inner cross area of the blood vessel is partially covered by an unsaturated lipid which is more permeable than the the inner surface of the normal artery. In this case, the slip velocity is more significant but its influence is not so effective due to the small passage of the arterial cross section which restricted the blood flow. Hence, with atherosclerosis, the flow region of the blood vessel reduces and restricts smooth flow. Additionally, a similar process is observed for nanoparticle dispersion. The stress-jump condition is considered at the interface of the clear region (defined by Herschel-Bulkley fluid) and peripheral region (defined by Newtonian fluid). The condition is more effective due to the change in the rheology of the fluid at different regions. With an increase in the stress-jump condition, the shear stress at the peripheral region is comparatively higher than at the clear region. With higher shear stress, the flow in the normal direction is restricted and reduces the dispersion phenomena presented by relative effective dispersion. The stress-jump condition significantly influences the relative effective dispersion; it helps in reducing relative effective dispersion for all values of n (see figure 3.5). It is noted that the changes are much more significant for $n = 1$, which represents Bingham fluid at the clear region which is basically similar to Newtonian fluid in the absence of the yield stress. These graphs also confirms the importance of the rheology of the fluid.

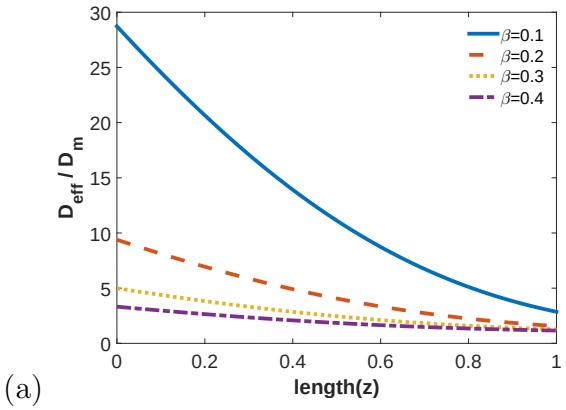

(a)

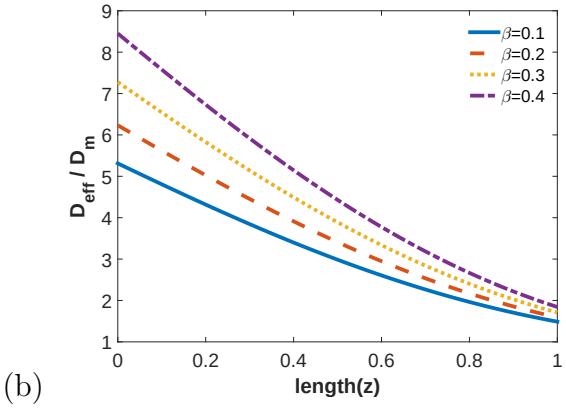

(b)

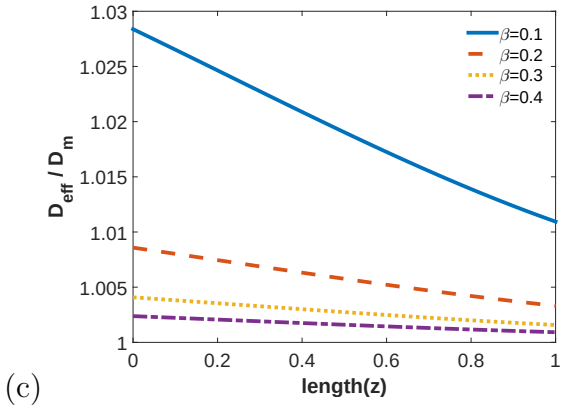

(c)

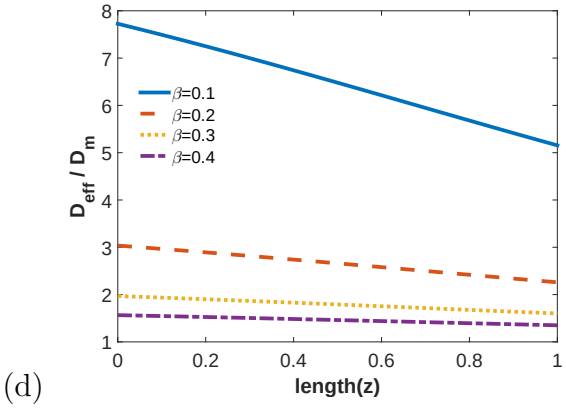

(d)

Figure 3.5: Relative effective dispersion vs axial direction for different stress jump constants when (a) $n = 0.5$, (b) $n = 2/3$, (c) $n = 1$ and (d) $n = 3/2$.

The rheological parameter represents the ratio between the plug region and the radius of the microvessel. Physically it depends on the volume fraction of the RBCs or hematocrit. The rheological parameter is proportional to the radius of the plug region where blood velocity is constant and the system behaves as a semisolid cylinder of RBCs. With an increase in the rheological parameter, the height of the plug region increases which reduces the gap between the plug region and the peripheral region. Practically, the nanoparticles do not get enough space for movement (Brownian motion) and hence reduces the dispersion near to the surface. The impact is more significant for a smaller value of the rheological parameter with the same difference (see figure 3.6). When nanoparticles are injected into the blood flow they spread across the vessel under the combined effect of diffusion and fluid flow (Shaw et al. [42]). Furthermore, the tumbling motion of RBCs influences the diffusion of solutes from the core region towards the edge, and along the axial direction. In addition, the axial tumbling and interaction of RBCs, solutes lead to deformation of the RBCs, thus a decrease in rotation or tumbling of RBCs, and a reduction in solute dispersion.

The permeability constant Π is critical in the dispersion characteristics of the nanoparticles displayed by Figure 3.7. The permeability nature of the wall of the microvessel is defined by Darcy's law. Closer to the surface endotheliam layer is a important factor, also works as a permeable barrier (Sugihara-Seki and Fu [46]). However, the permeability of the microvessel is different for different organs and their levels. The permeability parameter is smaller for the brain and higher for the glomerulus of kidney. It can be written in ascending order as, brain $<$ skin $<$ skeletal muscle $<$ lung $<$ heart $<$ gastrointestinal tract $<$ glomerulus of kidney (Deccuzzi et al. [7]). An observation is made where the dispersion of the nanoparticle is higher for larger values of the permeability parameters. Said another way, the dispersion of the nanoparticles during drug delivery is larger for the glomerulus of kidney and smaller for the brain. Endothelial permeability plays a vital role in preventing atherosclerosis. It is observed that the enhanced endothelial permeability leading to intimal accumulation of low-density lipoproteins (LDL) stimulates the formation of atherosclerotic lesions (Rozenberg et al. [37]). Clearly the dispersion of drug particles (nanoparticles) is higher at the tumor region during atherosclerosis. An opposite phenomena observed for $n = 1$, Bingham fluid, is shown in Figure 3.7c.

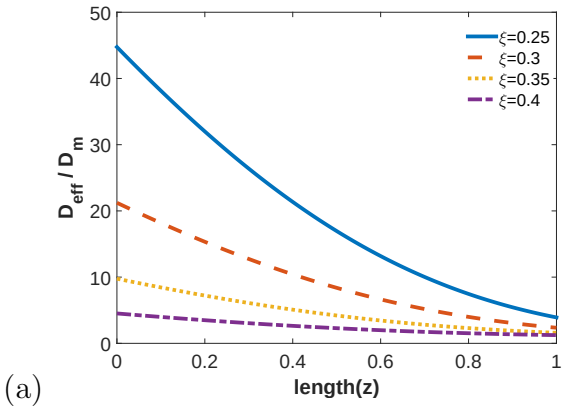

(a)

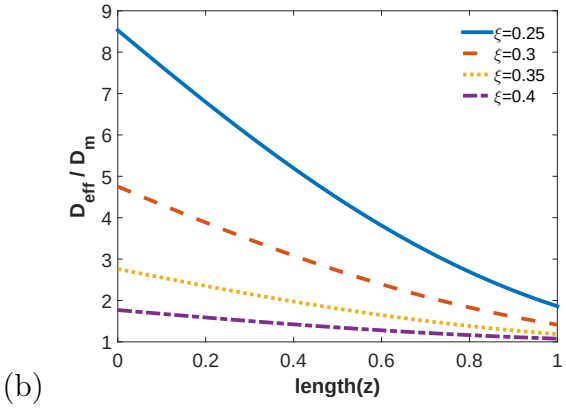

(b)

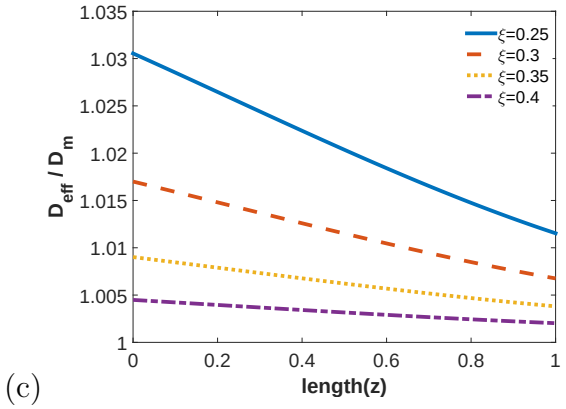

(c)

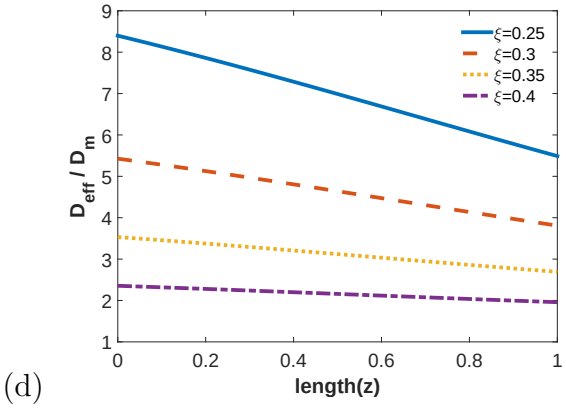

(d)

Figure 3.6: Relative effective dispersion vs axial direction for different rheological parameter when (a) $n = 0.5$, (b) $n = 2/3$, (c) $n = 1$ and (d) $n = 3/2$.

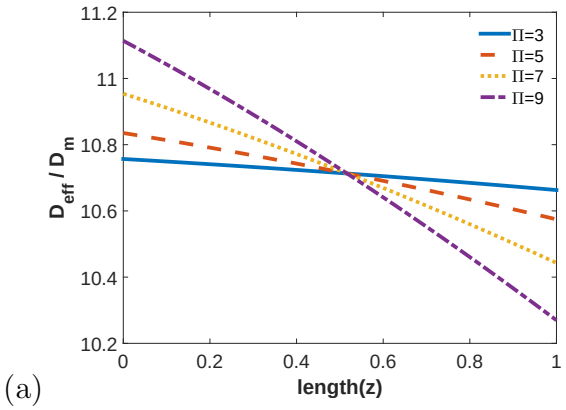

(a)

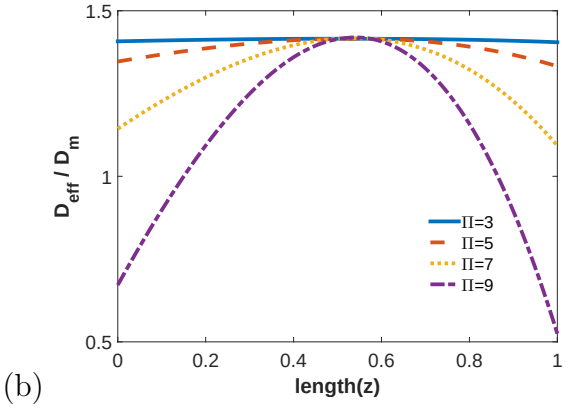

(b)

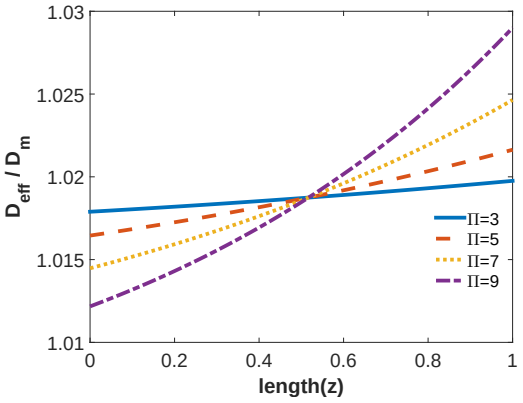

(c)

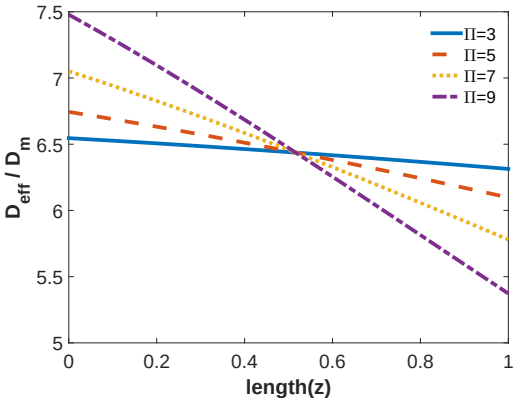

(d)

Figure 3.7: Relative effective dispersion vs axial direction for different permeability parameter when (a) $n = 0.5$, (b) $n = 2/3$, (c) $n = 1$ and (d) $n = 3/2$.

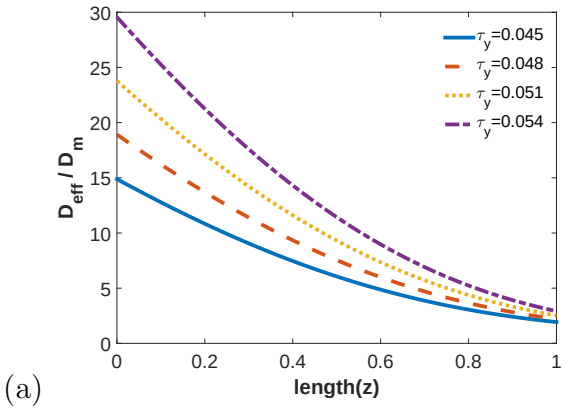

(a)

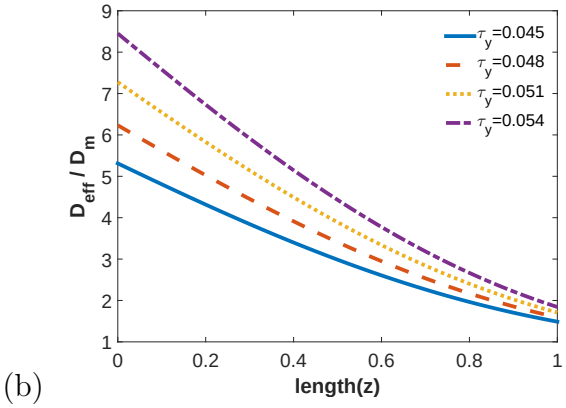

(b)

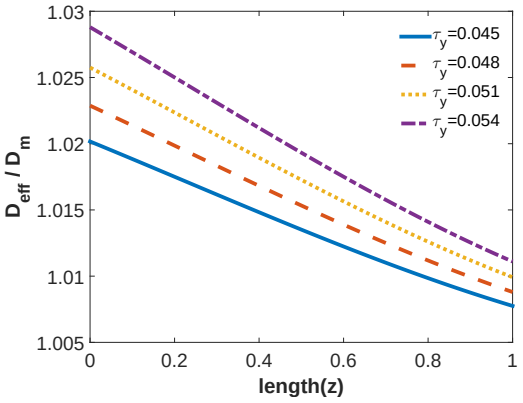

(c)

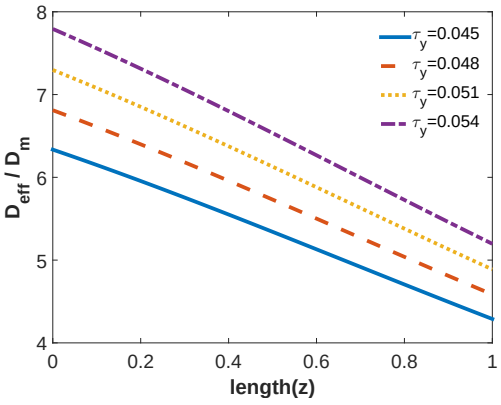

(d)

Figure 3.8: Relative effective dispersion vs axial direction for different yield stress when (a) $n = 0.5$, (b) $n = 2/3$, (c) $n = 1$ and (d) $n = 3/2$.

The yield stress is inversely proportional to the height of the core region as well as the pressure gradient. In the human body for a fixed vessel, the pressure gradient is a constant component so, with an increase in the yield stress there is a decrease in the height of the plug region. 3.8 shows that relative dispersion increases with an increase in the yield stress.

Conclusion

In this chapter we have studied the impact of the dispersion characteristics of nanoparticles during drug delivery. The blood flow through a microvessel was considered as a two-phase model where the core region is defined by a non-Newtonian Herschel-Bulkley fluid and the peripheral region is defined by a Newtonian fluid. The inner surface of the microvessel was considered as permeable in nature and defined by Darcy's model. The effect of the rheological parameter, the non-dimensional pressure constant, the nanoparticle volume fraction, the permeability parameter, the slip constant, the stress jump constant and the yield stress on the nanoparticle dispersion were analysed. From the above findings, one can conclude that the stress jump condition at the interface reduces the dispersion characteristics. A similar phenomenon follows with the rheological parameter. Permeability and yield stress enhanced the dispersion of nanoparticle at the inlet. With this work one gets an overall idea of the dispersion of solutes in blood flow under certain conditions which may help in drug delivery and the treatment of the cardiovascular disorders.

Chapter 4

Usteady solute dispersion in Herschel-Bulkley Fluid through a mild stenosed artery

4.1 Introduction

Studying solute dispersion in fluid flow is a captivating research topic due to its abundant applications in the fields of: chemical engineering (e.g chromatographic separation), Biomedical engineering (e.g transportation of drugs or toxins in physiological systems), environmental engineering (e.g pollutant transport) etc. Taylor [48] was the first to analyse the dispersion of solutes in laminar viscous fluids flow through a straight tube. In the study Taylor [48] defined D_{eff} (effective molecular diffusion coefficient) by $D_{eff} = \frac{R^2 w^2}{48 D_m}$ where R is the radius of the tube and w_m is molecular diffusivity. He went on to eaplain that solutes disperse due to radial molecular diffusion and axial convection. Later Aris [2] extended Taylor's dispersion concept by using the method of moments and defined effective molecular diffusivity(D_{eff}) as: $D_{eff} = D_m + \frac{R^2 w^2}{48 D_m}$. These two concepts however have to be extended since it only worked for large times after solutes have been injected into the fluid, that is when Gill and Sankarasubramanian [13] developed a generalized dispersion model that accounts for small and large times after solutes are injected into the fluid. Gill and Sankarasubramanian [40] later extended the analysis by showing that the three effective transport coefficients namely: exchange coefficient (K_0), convection

coefficient (K_1) and Dispersion coefficient (K_2) are influenced by interphase transport. The exchange coefficient arises due to the wall reaction at the boundary, the convection coefficient arises due to velocity of the solute and dispersion coefficient arises due to the molecular diffusion and the velocity of the fluid, Nagarani et al. [20].

The genereralized dipersion model brought a significant improvement into the study of fluid dynamics. Many researchers adapted Taylor-Aris's concept and the generalized dispersion model by Gill and Sankarasubramanian [40], to solve steady and unsteady flow problems of Newtonian and non-Newtonian fluids mostly in phisiogical systems. Nanda and Mallik [25] pointed out that blood behaves like a Newtonian fluid in large blood vessels and like a non-Newtonian in small vessels. Based on Taylor-Aris's concept Sharp [41] analysed the fully developed steady flow of non-Newtonian fluid and Gentile et al. [12] still on steady flow, analysed transport of nanoparticles in the blood vessels. Ganguly et al. [42] analysed the dispersion characteristics of blood during a nanoparticle assited drug delivery process through a permeable microvessel based on Taylor's theory of shear dispersion independent of time. Nagarani et al.([20]- [24]) studied unsteady solute dispersion in casson fluid flow, using generalized dispersion model. Rana and Murthy [34] studied axial solute dispersion in Carreau and Carreau-Yasuda fluid flows through a circular tube by considering boundary absorption/reaction at the tube wall. However in studies Nagarani et al.([20], [21], [24]) and, Rana and Murthy [34] revealed that blood flow is pulstile in nature with the same frequancy as the heartbeat. Following the generalized dispersion model Rana and Murthy [33] studied usteady solute dispersion in pulstile casson fluid flow in a tube with wall absorption. Later the study was extended and they analysed unsteady solute dispersion in small blood vessels using two phase casson model [36]. Nagarani et al [22] studied the dispersion of a solute in a pulstile non-Newtonian fluid (Casson fluid) through a tube. Over the years researchers have used the Casson and the Herchel-Bulkely model to describe the nature of blood rheology but according to information gathered, using the Herchel-Bulkely model describes blood closely and possesses more advantages compared to casson model. Scott (1996) and Sankar (2016) explained that the Herchel-Bulkely fluid model is more general for blood flow and it is easy to use and explain. Tu and Deville (1996) pointed out that the Herchel-Bulkely fluid model is more advantages since it can be reduced to the Newtonian, power-law and Bingham fluid models simply by change of parameters. Therefore using Herchel-Bulkely fluid model is a perfect choice describing blood rheology. According to the knowledge of the authors, analysis of unsteady solute dispersion modeling blood as Herchel-Bulkely fluid, considering the fact that blood

flow is pulstile in nature was studied by a few.

In the present paper we analyse the effects of wall absorbtion and yield stress on unsteady solute dispersion taking blood to behave like an Herchel-Bulkely fluid, considering the fact that blood flow is pulsatile in nature through a mild stenosed artery, using perturbation method used by Nagarani and Sarojamma [19] and the generalized dispersion model proposed by Gill and Sankarasubramanian ([40] [13]).

4.2 Mathematical formulation

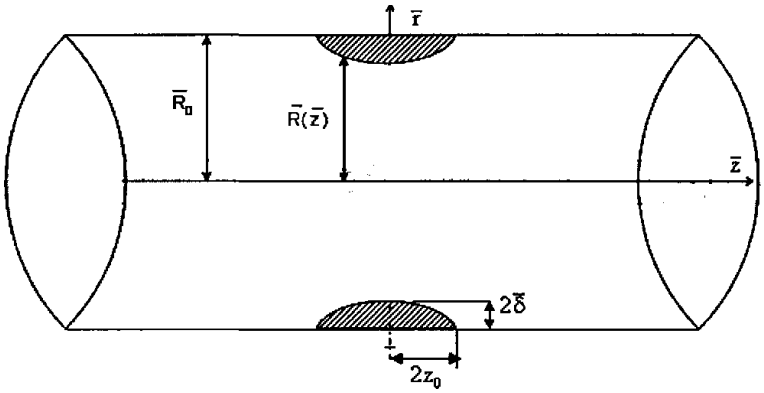

Figure 4.1: Schematic diagram of the stenosed artery

Let us consider a fully developed laminar of Herchely Bulkley flow,axially symmetric and pulstile blood flow in the presence of externally imposed periodic body acceleration in an artery with mild stenosis as shown in Fig.1. Following the stenotic protuberance used by Young [50], it is assumed to be axisymmetric surface generated by a cosine curve and the geometry of the stenosis is given by

$$\bar{R}(\bar{z}) = \begin{cases} R_0 - \bar{\delta}\big(1 + \cos\frac{\pi\bar{z}}{2\bar{z}_0}\big), & \text{for } \bar{z} = -2\bar{z_0} \;\; to \;\; \bar{z} = 2\bar{z_0}, \\ R_0, & \text{otherwise }, \end{cases} \tag{4.1}$$

where $\bar{R}(\bar{z})$ is the radius of the obstructed artery, R_0 is the the radius of a normal artery, $4\bar{z}$ is the length of the stenotic region and $2\bar{\delta}$ is the maximum proturberance of the stenotic at the artery wall. The periodic body acceleration in axial direction is given by

$$F(\bar{t}) = a_0 \cos(\omega_b \bar{t} + \phi), \tag{4.2}$$

where a_0 is the amplitude, $\omega_b = 2\pi f_b$,f_b is the frequency in Hz. The frequency of body acceleration f_b is assumed to be small so that the wave effect can be neglected and ϕ is the

lead angle of $F(\bar{t})$ with respect to the heart action. The pressure gradient is represented as follows

$$-\frac{\partial \bar{p}}{\partial \bar{z}} = P_0 + P_1 \cos(\omega_p \bar{t}), \tag{4.3}$$

where P_0 is steady component of the pressure gradient, P_1 is the fluctuating component, $\omega_p = 2\pi f_p$, f_p is the frequency of the pressure pulsation and $\bar{t}$ is time. The momentum equation is given as

$$\rho \frac{\partial \bar{w}}{\partial \bar{t}} = -\frac{\partial \bar{p}}{\partial \bar{z}} - \frac{1}{r}\frac{\partial}{\partial \bar{r}}(\bar{r}\bar{\tau}) + F(\bar{t}), \tag{4.4}$$

where ρ is the density, $\bar{\tau}$ and $\bar{w}$ are dimensional shear stress and velocity of the fluid respectively. Following Rana and Murthy [35] the constitutive equation for a Herschel-Bulkley fluid in one dimensional shear flow is given by

$$\bar{\tau} = \bar{\tau}_y + \eta_H \left(-\frac{\partial \bar{w}}{\partial \bar{r}} \right)^n \quad \text{if} \quad \bar{\tau} \geq \bar{\tau_y}, \tag{4.5}$$

$$\frac{\partial \bar{w}}{\partial \bar{r}} = 0 \quad \text{if} \quad \bar{\tau} \leq \bar{\tau_y}, \tag{4.6}$$

where $\bar{\tau}$ and $\dfrac{\partial w}{\partial r}$ are the shear stress and shear rate, respectively and τ_y is the yield stress, η_H is the viscosity of the Herschel-Bulkley fluid with dimension and n is the power-law index. Following boundary conditions taken into consideration

$$\bar{w} = 0 \quad \text{at} \quad \bar{r} = R(\bar{z}), \qquad \bar{\tau} \quad \text{is finite for} \quad \bar{r} = 0. \tag{4.7}$$

Non-dimensional Variables

$$C = \frac{\bar{C}}{C_0}, \quad w = \frac{\bar{w}}{w_0}, \quad r = \frac{\bar{r}}{R_0}, \quad z = \frac{D_m \bar{z}}{w_0 R_0^2}, \quad e = \frac{P_1}{P_0}, \quad a_1 = \frac{a_0}{P_0},$$
$$t = D_m \frac{\bar{t}}{R_0^2}, \quad \tau = \frac{\bar{\tau}}{\eta_0}\frac{R_0}{w_0}, \quad \tau_y = \frac{\bar{\tau}_y}{\eta_0}\frac{R_0}{w_0}, \tag{4.8}$$

where $w_0 = P_0\left(R_0^2/4\eta_0\right)$ and $\eta_0 = \eta_H \left(\dfrac{w_0}{R_0}\right)^{n-1}$, is the charecteristic viscosity.

4.2.1 Velocity distribution

Using non-dimentional variables, the momentum equation(4.4) becomes

$$\alpha^2 \frac{\partial w}{\partial t} = 2p(t) - \frac{1}{r}\frac{\partial}{\partial r}(r\tau) \tag{4.9}$$

where $\alpha^2 = D_m \rho/\eta_0$, $\quad p(t) = 2\left[1 + e\cos\left(\omega_p \dfrac{R_0^2}{D_m} t\right) + a_1 \cos(\omega_b \dfrac{R_0^2}{D_m} t + \phi)\right]$,

The non-dimensional form of equation (4.5) and (4.6) for a Herschel-Bulkley fluid is given as

$$\tau = \tau_y + \left(- \frac{\partial w}{\partial r} \right)^n \quad \text{if} \quad \tau \geq \tau_y, \tag{4.10}$$

$$\frac{\partial w}{\partial r} = 0 \quad \text{if} \quad \tau \leq \tau_y. \tag{4.11}$$

The boundary conditions (4.7) becomes

$$w = 0 \quad \text{at} \quad r = R(z), \qquad \tau \quad \text{is finite for} \quad r = 0. \tag{4.12}$$

The non-dimensional form of equation (4.1), geometry of the stenosis is given as

$$\bar{R}(\bar{z}) = \begin{cases} R_0 - \delta\left(1 + \cos\dfrac{\pi z}{2z_0}\right), & \text{for } z = -2z_0 \text{ to } z = 2z_0, \\ 1, & \text{otherwise .} \end{cases} \tag{4.13}$$

Using the perturbation analysis, equation (4.9)-(4.11) can be solved, the velocity w, shear stress τ, plug core radius R_p and plug core velocity w_p are expanded as follows in terms of α^2(where α^2 is very small and considered a perturbation parameter)

$$w(z, r, t) = w_0(z, r, t) + \alpha^2 W_1(z, r, t), \tag{4.14}$$

$$\tau(z, r, t) = \tau_0(z, r, t) + \alpha^2 \tau_1(z, r, t), \tag{4.15}$$

$$R_p(z, r, t) = R_{0p}(z, r, t) + \alpha^2 R_{1p}, \tag{4.16}$$

$$w_p(z, r, t) = w_{0p}(z, r, t) + \alpha^2 w_{1p}. \tag{4.17}$$

Substituting equation (4.14) and (4.15) into (4.9) and equating the constant terms and α^2 terms we get

$$\frac{\partial w_0}{\partial t} = \frac{1}{r}\frac{\partial}{\partial r}(r\tau_1), \tag{4.18}$$

$$2p(t) = \frac{1}{r}\frac{\partial}{\partial r}(r\tau_0). \tag{4.19}$$

Integrating equation (4.9) and using fact that τ is finite, we get

$$\tau_0 = p(t)r. \tag{4.20}$$

Substituting equation (4.14) and (4.15) into (4.10) we get

$$-\frac{\partial w_0}{\partial r} = (\tau_0 - \theta)^{1/n}, \tag{4.21}$$

$$-\frac{\partial w_1}{\partial t} = \frac{\tau_1}{n}(\tau_0 - \theta)^{1/n-1}. \tag{4.22}$$

where $\theta = \tau_y$, Using equation (4.20) and integrating (4.21) we get

$$w_0(r) = (p(t))^{1/n}\left(\frac{n}{n+1}\right)\left[(r-k^2)^{1/n+1} - (R-K^2)^{1/n+1}\right], \tag{4.23}$$

where $k^2 = \theta/p(t)$. At $r = R_{0p}$ we get plug core velocity w_{0p} as

$$w_{0p} = (p(t))^{1/n}\left(\frac{n}{n+1}\right)\left[(R_{0p}-k^2)^{1/n+1} - (R-K^2)^{1/n+1}\right] \tag{4.24}$$

where R_{0p} is the dimensionless radius of the plug region and neglecting the terms of $o(\alpha^2)$ and higher powers of α in Eq. (4.16) we get $R_{0p} = \theta/p(t)$. We get w_1 by integrating Eq. (4.22) and substituting it into Eq. (4.20), we get

$$\begin{aligned} w_1(r) \quad &= \sigma(t)\Bigg[R_{n4}(r-k^2)^{2/n-2} - \frac{R_n}{n}\Big(R_{n1}(r-k^2)^{1/n-2} - R_{n2}(r-k^2)^{1/n-3}\Big) \\ &\quad -\frac{n}{1-n}I_1(r) - R_{n3}(r-k^2)^{1/n-2}\Bigg], \end{aligned} \tag{4.25}$$

where $p_n(t) = p(t)^{1/n-1}$ and when $r = R_{0p}$ we get

$$\begin{aligned} w_{1p} \quad &= \sigma(t)\Bigg[R_{n4}(R_{0p}-k^2)^{2/n-2} - \frac{R_n}{n}\Big(R_{n1}(R_{0p}-k^2)^{1/n-2} - R_{n2}(R_{0p}-k^2)^{1/n-3}\Big) \\ &\quad -\frac{n}{1-n}I_1(R_{0p}) - R_{n3}(R_{0p}-k^2)^{1/n-2}\Bigg], \end{aligned} \tag{4.26}$$

Where $R_n, R_{n1}, R_{n2}, R_{n3}, R_{n4}, I_1(r)$ are found in the appendix.

4.2.2 Dispersion Distribution

The dispersion of the solute is governed by the unsteady convection diffusion equation below

$$\frac{\partial \bar{C}}{\partial \bar{t}} + \bar{w}\frac{\partial \bar{C}}{\partial \bar{z}} = D_m\left(\frac{1}{\bar{r}}\frac{\partial}{\partial \bar{r}}\left(\bar{r}\frac{\partial \bar{C}}{\partial \bar{r}}\right) + \frac{\partial^2 \bar{C}}{\partial \bar{z}^2}\right), \tag{4.27}$$

where D_m is the molecular diffusivity and $C(\bar{t}, \bar{z}, \bar{r})$ is the local concentration of the solute.

Initial and Boundary conditions

$$\bar{C}(0,\bar{z},\bar{r}) = C_0\psi(\bar{z})Y(\bar{r}), \tag{4.28}$$

$$C_0 = M/(\pi R^2), \quad \psi(\bar{z}) = \delta(\bar{z})R, \quad Y(\bar{r}) = 1, \tag{4.29}$$

$$\frac{\partial \bar{C}}{\partial \bar{r}}(\bar{t},\bar{z},0) = 0, \tag{4.30}$$

$$-D_m\frac{\partial \bar{C}}{\partial \bar{r}}(\bar{t},\bar{z},R) = k_c\bar{C}(\bar{t},\bar{z},R), \tag{4.31}$$

$$\bar{C}(\bar{t},\infty,\bar{r}) = \frac{\partial \bar{C}}{\partial \bar{z}}(\bar{t},\infty,r) = 0, \tag{4.32}$$

where $\bar{C}(0,\bar{z},\bar{r}) = C_0\psi(\bar{z})Y(\bar{r})$, $C_0 = M/(\pi R^2)$, and k_c is the reaction rate constant

Using non-dimensionless variables, Eq.(4.27) transforms to

$$\frac{\partial C}{\partial t} + w\frac{\partial C}{\partial z} = D_m\left(\frac{1}{r}\frac{\partial}{\partial r}\left(r\frac{\partial C}{\partial r}\right) + \frac{\partial^2 C}{\partial z^2}\right), \tag{4.33}$$

where $Pe = R_0\dfrac{w_0}{Dm}$ is the Peclet number. The initial and boundary condition becomes

$$C(0,z,r) = \psi(\{z)Y(r), \tag{4.34}$$

$$\frac{\partial C}{\partial r}(t,z,0) = 0, \tag{4.35}$$

$$\frac{\partial C}{\partial r}(t,z,1) = -\beta C(t,z,1), \tag{4.36}$$

$$C(t,\infty,r) = \frac{\partial C}{\partial z}(t,\infty,r) = 0, \tag{4.37}$$

where $\psi(\bar{z}) = \delta(\bar{z})/Pe$, $Y(r) = 1$, $\beta = kR_0/D_m$ is the wall absorption parameter.

To solve equation (4.33) we follow the method suggested by Sankarasubramanian and Gill [40], the solute concentration $C(t,z,r)$ can be expanded in an infinite series as

$$C(t,z,r) = \sum_{i=0}^{\infty} f_i(t,r)\frac{\partial^i C_m(t,z)}{\partial z^i}, \tag{4.38}$$

where $C_m(t,z)$ is the dimensionless mean concentration, and is given as

$$C_m(t,z) = 2\int_0^1 rC(t,z,r)dr. \tag{4.39}$$

Multiplying Eq.(4.33) by 2r and integrating with respect to r from 0 to 1, Equation (4.33) becomes

$$\frac{\partial C_m}{\partial t} = \frac{1}{Pe^2}\frac{\partial^2 C_m}{\partial z^2} + 2\frac{C}{\partial r}(t,z,1) - 2\frac{\partial}{\partial z}\int_0^1 w(t,r)C(t,z,r)rdr. \tag{4.40}$$

Substituting equation (4.38) into (4.40) we get an infinite series

$$\frac{\partial C_m}{\partial t} = \sum_{i=0}^{\infty} K_i(t)\frac{\partial^i C_m(t,z)}{\partial z^i}, \tag{4.41}$$

where

$$K_i(t) = \frac{\delta_{i2}}{Pe^2} + 2\frac{\partial f_i}{\partial r}(t,1) - 2\int_0^1 f_{i-1}(t,r)w(t,r)rdr \qquad i = 0,1,2... \tag{4.42}$$

and δ_{i2} is the kronecker delta defined by

$$\delta_{ik} = \begin{cases} 1, & \text{if } i = k, \\ 0, & \text{if } i \neq k. \end{cases} \tag{4.43}$$

Due to significance only $K_0(t)$, $K_1(t)$ and $K_2(t)$, exchange coefficient, convection coefficient and dispersion coefficient respectively are considered. In that case equation (4.38) and (4.41) now finite series, are given as

$$C(t,z,r) = \sum_{i=0}^{2} f_i(t,r)\frac{\partial^i C_m(t,z)}{\partial z^i}, \tag{4.44}$$

$$\frac{\partial C_m}{\partial t} = \sum_{i=0}^{2} K_i(t)\frac{\partial^i C_m(t,z)}{\partial z^i}, \tag{4.45}$$

where

$$K_i(t) = \frac{\delta_{i2}}{Pe^2} + 2\frac{\partial f_i}{\partial r}(t,1) - 2\int_0^1 f_{i-1}(t,r)w(t,r)rdr, \qquad i = 0,1,2. \tag{4.46}$$

Substituting equation (4.44) and(4.45) into equation (4.33) and equating coefficients of $\frac{\partial^i C_m}{\partial z^i}$, we get a partial differential equation

$$\frac{\partial f_i}{\partial t} = \frac{1}{r}\frac{\partial}{\partial r}\left(r\frac{\partial f_i}{\partial r}\right) - w(t,r)f_{i-1} + \frac{1}{Pe^2}f_{i-2} - \sum_{i=0}^{i} K_n(t)f_{i-n}, \qquad \text{for } \; i = 0,1,2, \tag{4.47}$$

where $f_{-1} = f_{-2} = 0$

Deriving initial and boundary conditions for equation (4.47), we use equation (4.38) and (4.39) with initial and boundary conditions (4.34)-(4.37), we get

$$C_m(0,z) = 2\psi(z)\int_0^1 rY(r)dr, \tag{4.48}$$

$$f_0(0,r) = \frac{Y(r)}{2\int_0^1 rY(r)dr}, \tag{4.49}$$

$$f_i(0,r) = 0, \quad i = 1,2, \tag{4.50}$$

$$\frac{\partial f_i}{\partial r}(t,0) = 0, \quad i = 0,1,2, \tag{4.51}$$

$$\frac{\partial f_i}{\partial r}(t,1) = -\beta f_i(t,1), \quad i = 0,1,2, \tag{4.52}$$

$$C_m(\{t,\infty) = \frac{\partial C_m}{\partial z}(t,\infty) = 0. \tag{4.53}$$

Using equation (4.38) into (4.39) we get an additional condition

$$\int_0^1 r f_i(t,r)dr = \frac{1}{2}\delta_{i0}, \quad i = 0,1,2, \tag{4.54}$$

with the initial and boundary conditions the differential equation (4.47) can be solved using Sturm Louville Theory to get f_0, f_1, f_2, K_0, K_1 and K_2.

4.2.3 Estimation of $f_0(t,r)$ and $K_0(t)$

Let i=0 then equation (4.47) reduces to

$$\frac{\partial f_0}{\partial t} = \frac{1}{r}\frac{\partial}{\partial r}\left(r\frac{\partial f_0}{\partial r}\right) - K_0(t)f_0. \tag{4.55}$$

The initial and boundary condition are given in (4.49), (4.51) and (4.52), for i=0 (4.54) becomes

$$\int_0^1 r f_0(t,r)dr = \frac{1}{2}. \tag{4.56}$$

Using the following transformation (4.55) is made easier

$$f_0 = exp\big(-\int_0^t K_0(s)ds\big)g_0(t,r). \tag{4.57}$$

Reducing (4.55) to

$$\frac{\partial g_0}{\partial t} = \frac{1}{r}\frac{\partial}{\partial r}\left(r\frac{\partial g_0}{\partial r}\right). \tag{4.58}$$

Solving (4.58) and subtituting back into (4.57) and using the additional condition we get $f_0(t,r)$ as

$$f_0(t,r) = \frac{\sum_{i=0}^{\infty} A_i J_0(\mu_i r) e^{-\mu_i^2 t}}{\sum_{i=0}^{\infty} (A_i/\mu_i) J_1(\mu_i) e^{-\mu_i^2 t}}, \tag{4.59}$$

where $\mu_i (i =, 1, 2...)$ are the roots of the transcendental equation $\mu_i J_1(\mu_i) = \beta J_0(\mu_i)$ and the constant A_i is given as

$$A_i = \frac{\mu_i^2 \int_0^1 rY(r) J_0(\mu_i r) dr}{(\mu_i^2 + \beta^2) J_0^2(\mu_i) \int_0^1 rY(r) dr}, \qquad i = 0, 1, 2.., \tag{4.60}$$

The exchange coefficient is independent of velocity field and $K_0(t)$ is given as

$$K_0(t) = 2\frac{\partial f_i}{\partial r}(t,1) = -2\beta f_0(t,1)) = \frac{\sum_{i=0}^{\infty} A_i - \mu_i J_1(\mu_i) e^{-\mu_i^2 t}}{\sum_{i=0}^{\infty} (A_i/\mu_i) J_1(\mu_i) e^{-\mu_i^2 t}}. \tag{4.61}$$

4.2.4 Estimation of $f_1(t,r)$ and $K_1(t)$

Using equation (4.47) we get the governing equation for $f_1(r,t)$ by setting $n = 1$ and is given as

$$\frac{\partial f_1}{\partial t} = \frac{1}{r}\frac{\partial}{\partial r}\left(r\frac{\partial f_1}{\partial r}\right) - K_0 f_1 - \big(w(t,r) + K_1\big) f_0. \tag{4.62}$$

Initial and Boundary conditions

$$f_1(0,r) = 0, \tag{4.63}$$

$$\frac{\partial f_1}{\partial r}(t,0) = 0, \tag{4.64}$$

$$\frac{\partial f_1}{\partial r}(t,1) = -\beta f_1(t,1). \tag{4.65}$$

Additional condition

$$\int_0^1 r f_1(t,r) dr = 0. \tag{4.66}$$

Using Sturm–Liouville theory the solution for $f_1(t,t)$ satisfying the initial, boundary conditions and the additional condition is given as

$$f_1(r,t) = -\frac{\sum_{j=0}^{\infty} A_j e^{-\lambda_j^2 t} J_0(\lambda_j r) D_{mn}(t)}{2\sum_{i=0}^{\infty} (A_i/\mu_i) e^{-\mu_i^2 t} J_1(\mu_i)}, \tag{4.67}$$

where

$$D_{mn}(t) = \int_0^t e^{-\lambda_j^2 s} \gamma(s) ds, \tag{4.68}$$

$$A_i = \frac{\mu_i^2 \int_0^1 rY(r)J_0(\mu_i r)dr}{(\mu_i^2+\beta^2)J_0^2(\mu_i)\int_0^1 rY(r)dr}, \tag{4.69}$$

$$\gamma(s) = \sum_{i=1}^{\infty} A_i A_j \int_0^t e^{-(\mu_i^2-\lambda_j^2)s} M_{nm}(s)ds + \sum_{i=1}^{\infty} A_i A_j \int_0^t \frac{1}{2}(J_0^2(\mu_i)+J_1^2(\mu_i))F_1(t), \tag{4.70}$$

$$M_{nm}(s) = \int_0^1 rw(r,s)J_0(\mu_i r)J_0(\mu_j r)dr, \tag{4.71}$$

$$F_1(t) = \int_0^t k_1(s)ds = -2\frac{\sum_{i=1}^{\infty}\sum_{j=1}^{\infty} A_i(A_j^2/\lambda_j)e^{-\lambda_j^2 t}\int_0^t e^{-(\mu_i^2-\lambda_j^2)s}M_{nm}(s)ds J_1(\lambda_j)}{\sum_{i=1}^{\infty}\sum_{j=1}^{\infty} A_j^2(A_i/\mu_i)J_1(\mu_i)e^{-\mu_i^2 t}(J_0^2(\mu_i)+J_1^2(\mu_i))}. \tag{4.72}$$

From equation (4.46) the convection coefficient $K_1(t)$ is

$$K_1(t) = 2\frac{\partial f_1(1,t)}{\partial r}(1,t) - 2\int_0^1 rw(t,r)f_0(r,t)dr, \tag{4.73}$$

where

$$\frac{\partial f_1}{\partial t}(1,t) = \frac{\sum_{j=0}^{\infty} A_j e^{-\lambda_j^2 t}\lambda_j J_1(\lambda_j)D_{mn}(t)}{2\sum_{i=0}^{\infty}(A_i/\mu_i)e^{-\mu_i^2 t}J_1(\mu_i)}, \tag{4.74}$$

$$\int_0^1 rw(t,r)f_0(r,t)dr = \frac{\sum_{i=0}^{\infty} A_i e^{-\mu_i^2 t}\int_0^1 rw(r,t)J_0(\mu_i r)dr}{\sum_{i=0}^{\infty}(A_i/\mu_i)e^{-\mu_i^2 t}J_1(\mu_i)}. \tag{4.75}$$

4.2.5 Estimation of $f_2(t,r)$ and $K_2(t)$

Using equation (4.47) we get the governing equation for $f_2(r,t)$ by setting $n=2$ and is given as

$$\frac{\partial f_2}{\partial t} = \frac{1}{r}\frac{\partial}{\partial r}\left(r\frac{\partial f_2}{\partial r}\right) - K_0 f_2 - \big(w(t,r)+K_1\big)f_1 + \big(\frac{1}{Pe^2} - K_2\big)f_0. \tag{4.76}$$

Initial and Boundary conditions

$$f_2(0,r) = 0, \tag{4.77}$$

$$\frac{\partial f_2}{\partial r}(t,0) = 0, \tag{4.78}$$

$$\frac{\partial f_2}{\partial r}(t,1) = -\beta f_2(t,1). \tag{4.79}$$

Additional condition

$$\int_0^1 r f_2(t,r)dr = 0. \tag{4.80}$$

Using Sturm–Liouville theory the solution for $f_1(t,t)$ satisfying the initial, boundary conditions and the additional condition is given as

$$f_2(r,t) = -\frac{\sum_{k=0}^{\infty} A_k J_0(\beta_k r) P(t)}{2\sum_{i=0}^{\infty}(A_i/\mu_i)e^{-\mu_i^2 t}J_1(\mu_i)}, \tag{4.81}$$

where

$$P(t) = -\sum_{j=0}^{\infty} A_k A_j e^{-\beta_k^2 t}\int_0^t e^{-\beta_k^2 s}\Big[b(s)M_{jk}(s) + F_{\lambda_j}K(s)\Big]ds - \sum_{i=0}^{\infty} A_i A_k e^{-\mu_i^2 t}F_{\mu_i}F_2(t), \tag{4.82}$$

$$F_{\lambda_j} = \frac{(J_0^2(\lambda_j) + J_1^2(\lambda_j))}{2}, \quad F_{\mu_i} = \frac{(J_0^2(\mu_i) + J_1^2(\mu_i))}{2}, \tag{4.83}$$

$$F_2(t) \quad = \int_0^t \left(K_2 - \frac{1}{Pe^2}\right)ds, \tag{4.84}$$

$$M_{jk}(s) = \int_0^1 r w(s,r) J_0(\lambda_j r) J_0(\beta_k r) dr, \tag{4.85}$$

$$b(t) = -\int_0^t e^{-\lambda_j^2(t-s)}\gamma(s)ds, \tag{4.86}$$

$$\gamma(s) = \sum_{i=1}^{\infty} A_i A_j \int_0^t e^{-(\mu_i^2-\lambda_j^2)s}M_{nm}(s)ds + \sum_{i=1}^{\infty} A_i A_j \int_0^t \frac{1}{2}(J_0^2(\mu_i) + J_1^2(\mu_i))F_1(t). \tag{4.87}$$

From equation (4.46) we get dispersion coefficient $K_2(t)$ as

$$K_2(t) = \frac{1}{Pe^2} + 2\frac{\partial f_2(1,t)}{\partial r}(1,t) - 2\int_0^1 r w(t,r) f_1(r,t) dr, \tag{4.88}$$

where

$$\frac{\partial f_2(1,t)}{\partial r}(1,t) = -\frac{\sum_{k=0}^{\infty} A_k \beta_k J_1(\beta_k) P(t)}{\sum_{i=0}^{\infty}(A_i/\mu_i)e^{-\mu_i^2 t}J_1(\mu_i)}, \tag{4.89}$$

$$2\int_0^1 r w(t,r) f_1(r,t) dr = \frac{-2\sum_{k=0}^{\infty} A_k e^{-\lambda_j^2 t} D_{mn}\int_0^1 r w(t,r) f_1(r,t) dr(t)\int_0^1 r w(t,r) J_0(\lambda_j r) dr}{\sum_{i=0}^{\infty}(A_i/\mu_i)e^{-\mu_i^2 t}J_1(\mu_i)} \tag{4.90}$$

4.3 Results and Discussion

The dispersion process is described by the three transport coefficients: exchange coefficient (K_0), convection coefficient (K_1) and dispesion coefficient (K_2). In this study all the three are calculated analytically and only the exchange coefficient (K_0) and the convection coefficient (K_1) are analysed. Negative exchange coefficient ($-K_0$) is analysed following analysis by Sankarasubramanian and Gill [40], Rana and Murthy [33, 34, 36]. It should be noted that the negative exchange coefficient ($-K_0$) does not depend on velocity unlike other transport coefficient, it depends more on the wall absorption parameter (β) as it can be seen in equation (4.61). The convection coefficient (K_1) and the dispesion coefficient (K_2) both depend on the yield stress (τ_y). To accomodate for small and large absorption rate, range of $0-100$ was suggested by Sankarasubramanian and Gill [40], and, Rana and Murthy [33].

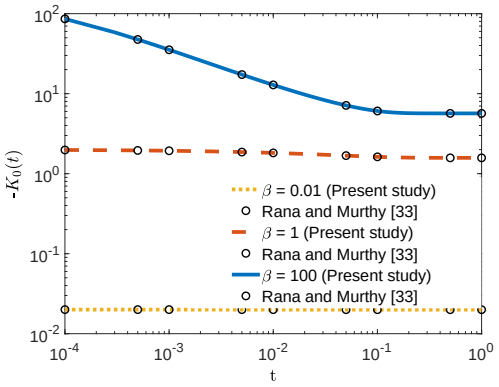

Figure 4.2: Negative exchange coefficient ($-K_0$) vs time for different value of wall absorption parameter (β) with a fixed flow index $n = 1/2$

A varying wall absorption parameter (β), $-K_0$ (negative exchange coefficient) with time variation is shown in Fig. 4.2. As β increases $-K_0$ increases, for small β the negative exchange coefficient ($-K_0$) is constant with time and low for large β value. The negative exchange coefficient ($-K_0$) is high and decreases with time after a long time $-K_0$ value becomes constant. This is the same for different values of n(flow index), this is because $-K_0$ is independent of velocity and pulsutility of the blood vessels hence independent of yield stress. A small value of the wall absorption parameter causes low reaction rate at the wall of the microvessel hence low $-K_0$ and as it increases $-K_0$ the reaction rate at the wall of a microvessel also increases.

Unlike the exchange coefficient (K_0), convectional coefficient depends on velocity, so it depends on β, τ_y, e, and the graphs below show how all these parameters affect the

negative convectional coefficient and results are discussed.

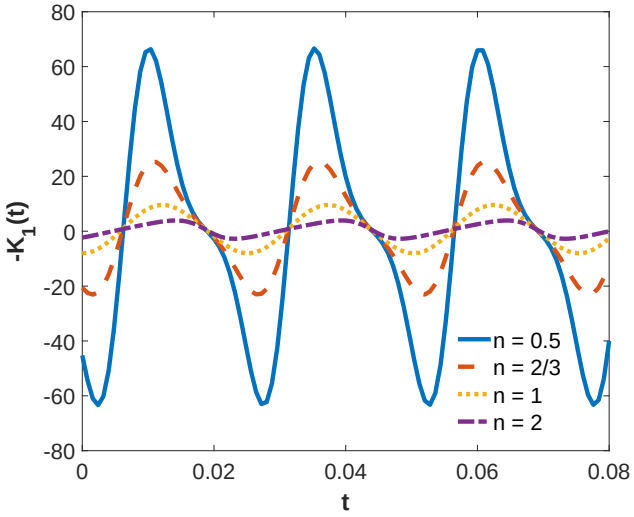

Figure 4.3: Negative convection coefficient $-K_1$ vs time t for different values of flow index n when $\tau_y = 0.05, e = 0.5, \beta = 0.01$

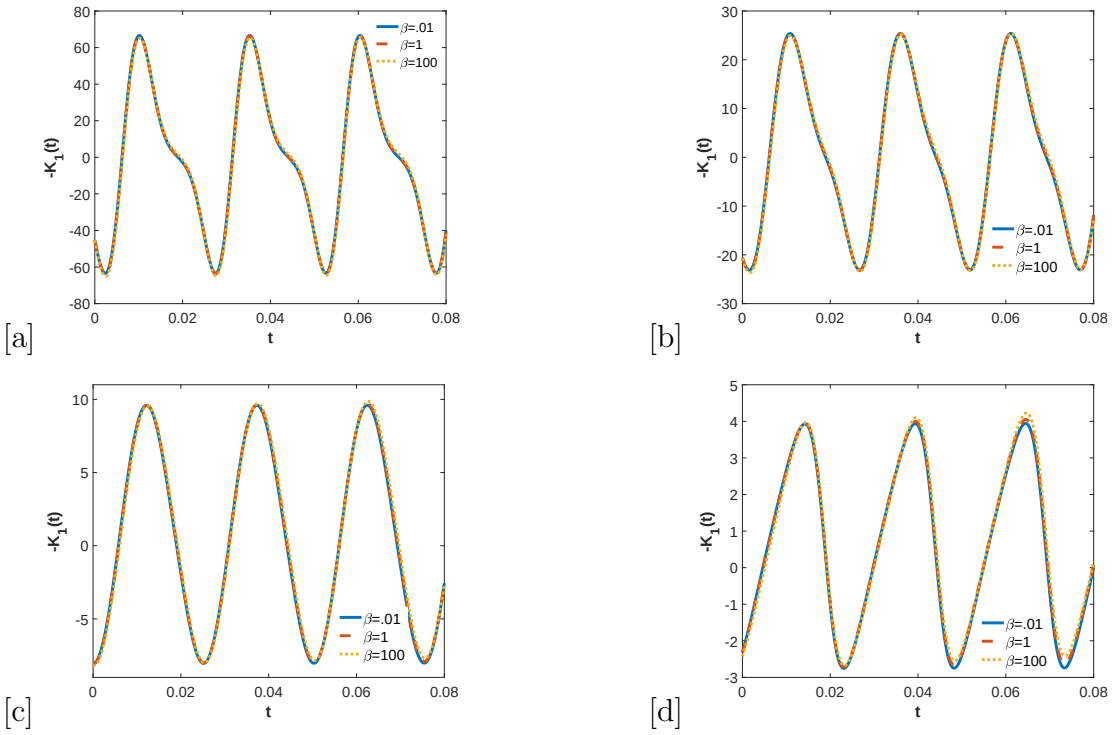

Figure 4.4: Negative convection coefficient $-K_1$ vs time t for different values of β when $n = 0.5, n = 2/3, n = 1, n = 2$ respectively

In Fig. 4.4(a-d) the variation of negative coefficient for small time is graphed for different values of β when $n = 0.5, n = 2/3, n = 1, n = 2$ (a-d), respectively. It is observed

that when n is less than 1, β increases $-K_1$ decreases and for n greater or equal to 1 $-K_1$ increases with β. The same results (of $-K_1$, increasing with β) were noticed by Rana and Murthy [33–35], this can be attributed to the shear thinning nature becoming more prominent in the fluid. Consequently, the velocity of the fluid increases so does $-K_1$. For n greater or equal to 1, it is noticed that as β increases the amplitude of the fluctuation and the magnitude of $-K_1$ increases and becomes stable after some time.

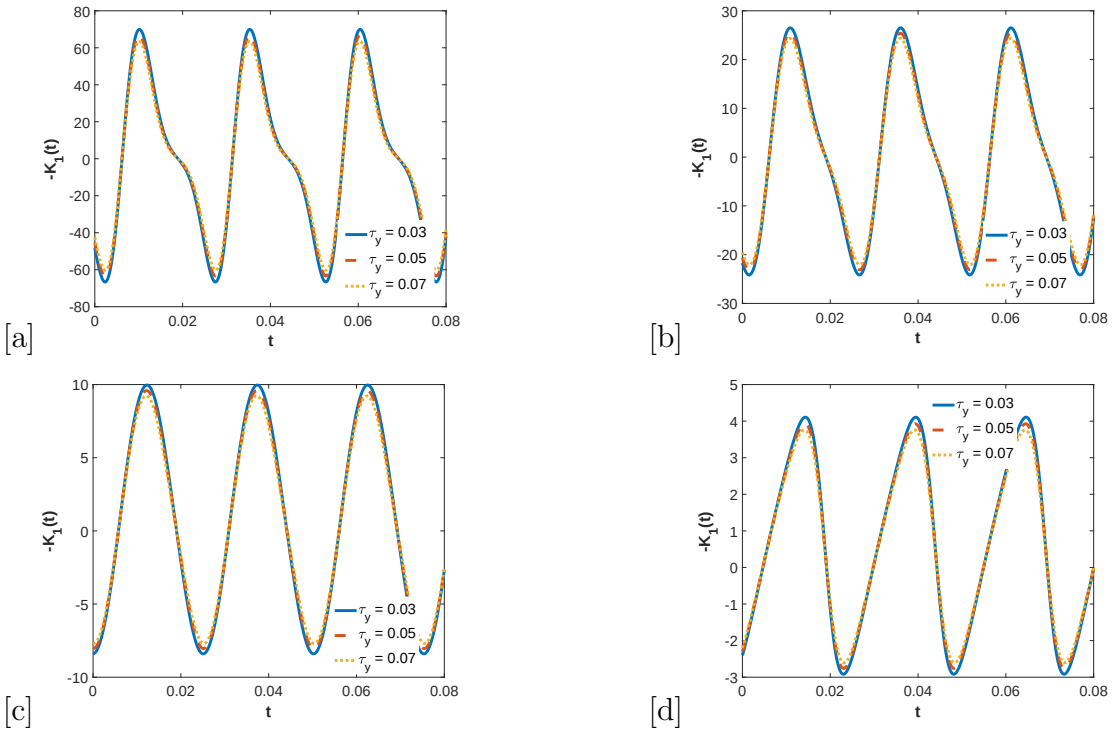

Figure 4.5: Negative convection coefficient $-K_1$ vs time t for different values of τ_y when $n = 0.5, n = 2/3, n = 1, n = 2$ respectively

In Fig. 4.5(a-d) the variation of negative coefficient for small time is graphed for different values of τ_y when $n = 0.5, n = 2/3, n = 1$ and $n = 2$, respectively. Results shows that for all n, τ_y there is a significant effect on $-K_1$. When τ_y increases $-K_1$ decreases, owing to the effect of τ_y on velocity, τ_y reduces velocity of the fluid hence solutes are convected at low fluid velocity. The same results were observed by Sankasubramanian and Gill [40], Rana and Murthy [35]

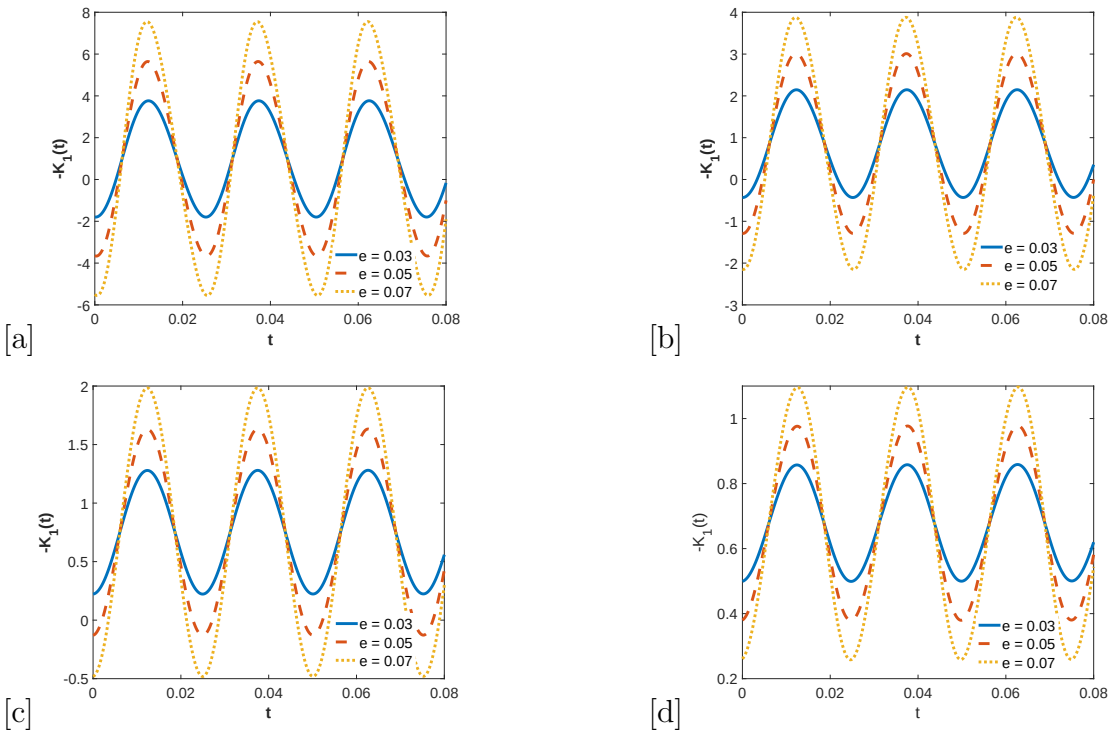

Figure 4.6: Negative convection coefficient $-K_1$ vs time t for different values of e when $n = 0.5, n = 2/3, n = 1, n = 2$ respectively

In Fig. 4.6 the variation of negative coefficient for small time is graphed for different values of e when $n = 0.5, n = 2/3, n = 1, n = 2$ (a-d) respectively. It is observed that when n increases $-K_1$ decreases, and it is also noticed that as e increases K_1 increases. This is because an increase in e increases the fluctuating pressure gradient hence the increase in the amplitude of fluid velocity leading to increase in $-K_1$ fluctuation Rana and Murthy [34].

4.4 Conclusion

In this study we analysed the effect of wall absorption and yield stress on the dispersion process in a mild stenosed artery, considering the flowing fluid as a Herschel-Bulkely fluid and looking at the pulsatile flow of blood under the influence of body acceleration. Three coefficients namely: exchange coefficient, convection coefficient and dispersion coefficient are calculated analytically and only two are analysed, that is the exchange coefficient and the convection coefficient. It is observed that the exchange coefficient K_0 is not affected by the motion of fluid i.e it is independent of fluid velocity, and is only affected by wall absorption. Unlike K_0, the convectional coefficient K_1 is affected by the velocity of the fluid hence a great significant effect of wall absorption β, yield stress τ_y and pulsatile pressure gradient e on K_1.

Chapter 5

Conclusion & Future Scope

5.1 Conclusion

The first chapter gives the basics and principles of bio-fluid dynamics. The second chapter is based on the study of velocity, temperature and the concentration of blood flow through a microvessel contain peripheral layer. The velocity and concentration profile are divided into three regions e.g., plug region, outer region and peripheral region. The influence of the stress jump condition, the slip condition of velocity and the concentration , the yield stress, the pressure gradient and the permeability of the peripheral region play crucial roles which are reflected through graphs. In general it is observed that the velocity and concentration at the plug region is constant while after that velocity decreases through out the radius but concentration increases continuously in radial direction. Velocity is non-zero at the walls of the microvessel because of the slip constantγ and the stress jump constant causes a rapid decrease in velocity between the core region and the peripheral region. Temperature profile is challenging for all the parameters. This work may give an overall idea of blood flow in the sense of velocity, temperature and concentration under certain condition.

The third chapter is based on the analysis of the effect of rheological parameter ,non-dimensional pressure constant, nanoparticle volume fraction, the slip constant, the stress jump constant, the permeability parameter and the yield stress on the nanoparticle dispersion has been analysed. From the above findings, one can conclude that relative effective dispersion is heavily affected by all these parameters. This works may give an overall idea of dispersion of solutes in blood flow and how it is affected by certain conditions.

In the forth chapter, we analyse the effect of wall absorption and yield stress on dispersion process in a mild stenosed artery, considering the flowing fluid as a Herschel-Bulkely fluid and looking at the pulsatile flow of blood under the influence of body acceleration. Three coefficients namely: the exchange coefficient, the convection coefficient and the dispersion coefficient are calculated analytically. And only two are analysed, that is exchange coefficient and convection coefficient. It is observed that the exchange coefficient K_0 is not affected by the motion of the fluid that is it is independent of fluid velocity hence it is only affected by wall absorption. And unlike K_0, the convectional coefficient K_1 is affected by the velocity of the fluid. So, a great significant effect of wall absorption β, yield stress τ_y and pulsatile pressure gradient e on K_1.

5.2 Future Scope

In the present thesis we mainly focus on the effect of blood rheological parameters (slip constant, stress jump constant, yield stress, wall absorption constant, non-dimensional pressure constant, nanoparticle volume fraction etc) on solutes dispersion through permeable microvessel and mild stenosed artery. Considering both steady and unsteady flow of Casson fluid and Herschel-Bulkely fluid. Furthermore, the present work can be extended as follows;

- The study of unsteady dispersion in a Herschel-Bulkely fluid through a mild stenosed artery with a pulsatile flow of blood under the influence of body acceleration which is in the forth chapter, can in future be extended by changing single mild stenosed artery to multi stenosed artery.

- Casson fluid and Herschel-Bulkely fluid model are widely used in bio-fluid, but in some special cases, Carreau and Carreau-Yasuda fluid model can be used since it also describes the behavior of the viscosity of blood at low and high shear rate regions.

- The artery of the cardiovascular system is not always shaped like a circular straight cylinder the shape depends on the position at different organs, it may be curved or bifurcated. In future, the present problem can be extended with the above mentioned complex geometries.

Bibliography

[1] Aris R.,1956. On the dispersion of a solute in a fluid flowing through a tube. Proc. R. Soc. Lond. A 235, 67–77.

[2] Aris R., 1960. On the dispersion of a solute in pulsating flow through a tube. Proc. R. Soc. Lond. A 259, 370–376.

[3] Brinkman, H.C., 1952. The viscosity of concentrated suspensions and solutions. The Journal of Chemical Physics, 20(4), 571-571.

[4] Bugliarello, G., Sevilla, J., 1970. Velocity distribution and other characteristics of steadyand pulsatile bloodflow infine glass tubes. Biorheology 7, 85–107.

[5] Chen,MM., Holmes, KR., 1980, contribution in tissue heat transfer, Annals of the NewYork Academic Sciences, 335 137-150.

[6] Das S, Chakraborty S.,2006. Analytical solutions for velocity, temperature and concentration distribution in electroosmotic microchannel flows of a non-Newtonian bio-fluid, Analytica Chimica Acta 559-1524.

[7] Decuzzi, P., Causa, F., Ferrari, M. and Netti, P.A., 2006. The effective dispersion of nanovectors within the tumor microvasculature. Annals of biomedical engineering, 34(4), 633-641.

[8] Einstein, A., 1906. A new determination of molecular dimensions. Ann. Phys., 19, 289-306.

[9] Fahraeus, R. and Lindqvist, T., 1931. The viscosity of the blood in narrow capillary tubes. American Journal of Physiology-Legacy Content, 96(3), 562-568.

[10] Fasano,A., Sequeira, A., 2017. Blood and Heat Transfer, Hemomath, 18, 227-264.

[11] Fullstone, G., Wood, J., Holcombe, M., Battaglia, G., 2014, Modellig the transport of nanoparticles under blood flow using an agent-based approach, Scientific Reports, 5, 10649

[12] Gentile,F., Ferrari,M., Decuzzi,P., 2008, The transport of nanoparticles in blood vessels: the effect of vessel permeability and blood rheology, Annals of Biomedical Engineering, 36, 254-261.

[13] Gill WN, Sankarasubramanian R., 1970. Exact analysis of unsteady convective diffusion. Proc. R. Soc. Lond. A 316, 341–350.

[14] Huang,H. W., Chan,C. L., Roemer,R. B. , 1994, Analytical solutions of pennes bioheat transfer equation with a blood vessel, J Biomech Eng, 116, 208-212.

[15] Khaled,ARA., Vafai,K., 2003, The role of porous media in modeling flow and heat transfer in biological tissues, International Journal of Heat and Mass Transfer, 46, 4989-5003.

[16] Mazumdar,JN .,1992. Biofluid Mechanics, World Scientific, First Edition.

[17] Misra,J.C., Adikari,S.D., 2016, oscillatory channel flow, heat and mass transfer in a physiological fluid in presence of chemical reaction, Alexandria Engineering Journal, 55, 287-297.

[18] Nallapu S, Radhakrishnamacharya G., 2014. Herschel-Bulkley Fluid Flow through Narrow Tubes, Central European Journal of Physics, 1-12.

[19] Nagarani, P. and Sarojamma, G., 2008. Effect of body acceleration on pulsatile flow of Casson fluid through a mild stenosed artery. Korea-Austrtralia Rheology Journal, 4, 189-196.

[20] Nagarani, P., Sarojamma, G., Jayaraman, G., 2004 Effect of boundary absorption in dispersion in Casson fluid flow in a tube. Ann. Biomed. Eng. 32, 706–719

[21] Nagarani, P., Sarojamma,G. and Jayaraman, G., 2009 Effect of boundary absorption on dispersion in Casson fluid flow in an annulus - application to catheterized artery, Acta Mechanica, 202, 47-63.

[22] Nagarani, P., Sebastian, B. T., 2013 Dispersion of a solute in pulsatile non-Newtonian fluid flow through a tube. Acta Mechanica. 224(3), 571–585.

[23] P. Nagarani, B.T. Sebastian, 2017 Effect of flow unsteadiness on dispersion in non-Newtonian fluid in an annulus. J. Appl. Math. Inform. 35 (3–4), 241-260

[24] Nagarani, P., Sebastian, B.T., 2018. Convection-diffusion in unsteady non-Newtonian fluid flow in an annulus with wall absorption. Korea-Australia rheology journal, 30(4), 261-271.

[25] Nanda, S.P., and Mallik, B.B., 2011. A mathematical analysis on blood flow through an artery with a branch capillary. Journal of Mechanics of Continua and Mathematical sciences, 6(1), 707-716.

[26] Pasol, L. and Feuillebois, F., 2004, August. Effective viscosity of an inhomogeneous dilute suspension flowing along a wall. In Proceedings of the 21st International Congress of Theoretical and Applied Mechnics, Warsaw, Poland, 15-21.

[27] Pennes, H.H., 1948, Analysis of tissue and arterial temperatures in the resting human forearm. J. Appl. Physiol., 1, 93-122.

[28] Ponalagusamy, R. and Tamil, S.R., 2015, Influence of magnetic field and heat transfer on two-phase fluid model for oscillatory blood flow in an arterial stenosis, Meccanica, 50, 927-943.

[29] Pries, A.R. and Secomb, T.W., 2005. Microvascular blood viscosity in vivo and the endothelial surface layer. American Journal of Physiology-Heart and Circulatory Physiology, 289(6), H2657-H2664.

[30] Ramana B. and G. Sarojamma., 2012. Effect of wall absorption on dispersion of a solute in a Herschel–Bulkley fluid through an annulus, Adv. Appl. Sci. Res. 3, 3878–3889.

[31] Ramana, B. and Sarojamma, G., 2012. Unsteady convective diffusion in a Herschel-Bulkley fluid in a conduit with interphase mass transfer: Int. J. Math. Model. Comput. 2, 159-179.

[32] Ramya, D., Raju, R.S., Rao, J.A. and Chamkha, A.J., 2018. Effects of velocity and thermal wall slip on magnetohydrodynamics (MHD) boundary layer viscous flow and heat transfer of a nanofluid over a non-linearly-stretching sheet: a numerical study. Propulsion and Power Research, 7(2), 182-195.

[33] Rana J, Murthy PVSN. 2016 Solute dispersion in pulsatile Casson fluid flow in a tube with wall absorption. J. Fluid Mech. 793, 877–914.

[34] Rana J, Murthy PVSN. 2016 Unsteady solute dispersion in non-Newtonian fluid flow in a tube with wall absorption, Proc. R. Soc. A 472, 2016-0294

[35] Rana J, Murthy PVSN. 2016 Unsteady solute dispersion in Herschel-Bulkley fluid in a tube with wall absorption. Phys. Fluids 28, 111903.

[36] Rana J, Murthy PVSN. 2017 Unsteady solute dispersion in small blood vessels using a two-phase Casson model. Proc. R. Soc. A 473, 2017-0427.

[37] Rozenberg, I., Sluka, H.M.S., Rohrer, L., Hofmann, J., Becher, B., Akhmedov, A., Soliz, J., Mocharla, P., Borén, J., Johansen, P., Steffel, J., Watanabe, T., Lüscher, T.F., Tanner, F.C., 2010, Histamine H1 receptor promotes atherosclerotic lesion formation by increasing vascular permeability for low-density lipoproteins, Arteriosclerosis, Thrombosis, and Vascular Biology, 30, 923-930.

[38] Sinha, A., .Misra, J.C., Shit, G.C., 2016. Effect of heat transfer on unsteady MHD flow of blood in a permeable vessel in the presence of non-uniform heat source, Alexandria Engineering Journal, 55, 2023-2033.

[39] Sinha, A., Shit, G.C., Kundu, P.K., 2013, Slip Effects on Pulsatile Flow of Blood through a Stenosed Arterial Segment under Periodic Body Acceleration, ISRN Biomedical Engineering, 2013, Article ID 925-876.

[40] Sankarasubramanian, R. and Gill, W.N., 1973. Unsteady convective diffusion with interphase mass transfer. Proceedings of the Royal Society of London. A. Mathematical and Physical Sciences, pp.115-132.

[41] Sharp, M.K., 1993. Shear-augmented dispersion in non-Newtonian fluids. Annals of biomedical engineering, 21(4), 407-415.

[42] Shaw, S., Ganguly, S., Sibanda, P., Chakraborty, S. 2014 Dispersion characteristics of blood during nanoparticle assisted drug delivery process through a permeable mirovessel. Microvasc. Res. 92, 25-33.

[43] Shaw, S., Murthy, P.V.S.N. and Sibanda, P., 2013. Magnetic drug targeting in a permeable microvessel. Microvascular research, 85, 77-85.

[44] Shaw, S., Murthy, P.V.S.N., 2010. Magnetic drug targeting in the permeable blood vessel - the effect of blood rheolgy, J of Nanotech. in Engng. and Medicine, 1, 021-001.

[45] Shaw, S., Murthy, P.V.S.N., 2010. Magnetic drug targeting in the impermeable microvessel with two phase fluid model — non-Newtonian characteristics of blood. Microvasc. Res. 80, 209–220

[46] Sugihara-Seki, M., Fu, B.M., 2005. Blood flow and permeability inmicrovessels. Fluid Dyn. Res. 37, 822-132.

[47] Sushma,S., Samuel, N., Neeraja,G., 2018, Slip flow effects on unsteady mhd blood flow in a permeable vessel in the presence of heat source/sink and chemical reaction, Global Journal of Pure and Applied Mathematics, 14, 1083-1099.

[48] Taylor G., 1953. Dispersion of soluble matter in solvent flowing slowly through a tube. Proc. R. Soc. Lond. A 219, 186–203.

[49] Xu, Z., Chen, N., Shadden, S.C., Marsden, J.E., Kamocka,M.M., Rosen,E.D., Alber,M., 2009, Study of blood flow impact on growth thrombi using a multiscale model, Soft Matter, 5, 769-779.

[50] Young, D. F., 1968, Effect of a time-dependent stenosis on flow through a tube, J. Engng. Ind. Trans. ASME 90, 248-254.

[51] Yue, K., Zhang, X., Yu, F., 2004, An Analytic Solution of One-dimensional Steady-state Pennes' Bioheat Transfer Equation in Cylindrical Coordinates , J. of Thermal Science, 13, 255-258.

APPENDIX

Chapter 2 Appendix

$\lambda^2 = \frac{-k}{\mu_2}$

$\kappa = \frac{1}{\mu_2}\frac{dp}{dz}$

$T_1 = \frac{h_2^2}{4\mu_1}\frac{dp}{dz} - \frac{h_2\tau_y}{\mu_1} + \frac{4h_2^{3/2}}{3\mu_1}\sqrt{\frac{-\tau_y}{2}\frac{dp}{dz}} - \frac{\kappa}{\lambda^2}$

$T_2 = \frac{h_2^2}{2\mu_1}\frac{dp}{dz} - \frac{\tau_y}{\mu_1} + \frac{2h_2^{1/2}}{\mu_1}\sqrt{\frac{-\tau_y}{2}\frac{dp}{dz}}$

$T_3 = \frac{h_1^2}{4\mu_1}\frac{dp}{dz} - \frac{h_1\tau_y}{\mu_1} + \frac{4h_1^{3/2}}{3\mu_1}\sqrt{\frac{-\tau_y}{2}\frac{dp}{dz}}$

$S_1 = -\mu_2\lambda J_0(\lambda h_2) - \mu_2\beta J_0(\lambda h_2)$

$S_2 = -\mu_2\lambda Y_1(\lambda h_2) - \mu_2\beta Y_0(\lambda h_2)$

$S_3 = \lambda J_1(\lambda h) - \gamma J_0(\lambda h)$

$S_4 = \lambda Y_1(\lambda h) - \gamma Y_0(\lambda h)$

$m_1 = (T_2 + \mu_2\beta\frac{\kappa}{\lambda^2} - \gamma\frac{\kappa}{\lambda^2}\frac{\S_1}{\S_3})(\frac{S_3}{S_1\S_4 + S_2\S_3})$

$m_2 = \gamma\kappa(\frac{S_3}{S_3^2\lambda^2 - m_2\S_4})$

$B = m_1 J_0(\lambda h_2) + m_2 Y_0(\lambda h_2) - T_1$

$G_1 = \frac{U_p}{D_m}\frac{dC}{dz}\frac{h_1^2}{4} - (\frac{h_1^4}{64\mu_1}\frac{dp}{dz} - \frac{h_1^3}{9}\frac{\tau_y}{\mu_1} + \frac{16}{147}\frac{h_1^{\frac{7}{2}}}{\mu_1}\sqrt{\frac{-\tau_y}{2}\frac{dp}{dz}} + \frac{Bh_1^2}{4})\frac{1}{D_m}\frac{dC}{dz}$

$G_2 = (\frac{m_1}{\lambda^2}J_0(\lambda h_2) - \frac{m_2}{\lambda^2}Y_0(\lambda h_2) + \frac{h_2^2}{4}\frac{\kappa}{\lambda^2})\frac{1}{D_m}\frac{dC}{dz} - (\frac{h_2^4}{64\mu_1}\frac{dp}{dz} - \frac{h_2^3}{9}\frac{\tau_y}{\mu_1} + \frac{16}{147}\frac{h_2^{\frac{7}{2}}}{\mu_1}\sqrt{\frac{-\tau_y}{2}\frac{dp}{dz}} + \frac{Bh_2^2}{4})\frac{1}{D_m}\frac{dC}{dz}$

$G_3 = (\frac{h_2^3}{16\mu_1}\frac{dp}{dz} - \frac{h_2^2}{3}\frac{\tau_y}{\mu_1} + \frac{8}{21}\frac{h_2^{\frac{5}{2}}}{\mu_1}\sqrt{\frac{-\tau_y}{2}\frac{dp}{dz}} + \frac{Bh_2}{2})\frac{1}{D_m}\frac{dC}{dz} + (\frac{m_1}{\lambda}J_1(\lambda h_2) + \frac{m_2}{\lambda}Y_1(\lambda h_2) + \frac{h_2}{2}\frac{\kappa}{\lambda^2})\frac{1}{D_m}\frac{dC}{dz}$

$G_4 = (\frac{m_1}{\lambda}J_1(\lambda h) + \frac{m_2}{\lambda}Y_1(\lambda h) + \frac{h}{2}\frac{\kappa}{\lambda^2})\frac{1}{D_m}\frac{dC}{dz} + \gamma(\frac{m_1}{\lambda^2}J_0(\lambda h) - \frac{m_2}{\lambda^2}Y_0(\lambda h) + \frac{h^2}{4}\frac{\kappa}{\lambda^2})\frac{1}{D_m}\frac{dC}{dz})$

$B_1 = (G_2 - h_2 G_3 lnh_2 + \frac{G_4}{\gamma} + \frac{1}{\gamma D_m}\frac{dC}{dz} + G_3 h_2 lnh + G_1)\frac{1}{lnh_1 - lnh}$

$B2 = G_1 - B_1 lnh_1$

$B_3 = G_3 h_2 + B_1$

$B_4 = -(\frac{G_4}{\gamma} + \frac{1}{\gamma D_m}\frac{dC}{dz} + B_3 lnh)$

$\tau_{yp} = \sqrt{\frac{-\tau_y}{2}\frac{dp}{dz}}$

$A_1 = B - U_{av}$

Working for equation (2.1) to (2.3)

Solving equation (2.1) to (2.3), we use the Casson model shown below

$\tau^{1/2} = \tau_y^{1/2} + \left(-\mu_1 \frac{\partial U_1}{\partial r} \right)^{1/2}$

Making $\frac{\partial U_1}{\partial r}$ the subject, the Casson model gives

$\frac{\partial U_1}{\partial r} = \frac{1}{\mu_1}\left(\tau - 2\sqrt{\tau\tau_y} + \tau_y \right)$

Using equation (2.2) on the above equation, we get

$\frac{\partial U_1}{\partial r} = \frac{r}{2\mu_1}\frac{dp}{dz} - \frac{\tau_y}{\mu_1} + \frac{2}{\mu_1}\sqrt{\frac{-r\tau_y}{2}\frac{dp}{dz}}$

Hence equation (2.9) when the above equation is integrated once. Using the boundary condition (2.5) we get (2.8). Furthermore, using the method of undetermined coefficient on the equation (2.7), it gives out equation (2.10)

Chapter 3 Appendix

$$T_1 = \frac{-1}{2\mu_1}\frac{\partial p}{\partial z}^{1/n}\frac{n}{n+1}(h_1 - h_p)^{1+1/n} + \frac{1}{4\mu_2}\frac{\partial p}{\partial z}h_1^2$$

$$\mathrm{T}_2 = \frac{-1}{2\mu_1}\frac{\partial p}{\partial z}^{1/n}(h_1 - h_p)^{1/n} + \frac{1}{2}\frac{\partial p}{\partial z}h_1 - \beta\frac{1}{4}\frac{\partial p}{\partial z}h_1^2$$

$$\epsilon = -\mu_2\beta, \quad \upsilon = \frac{\mu_2}{h_1}, \quad \eta = \epsilon \ln h_1, \quad \omega = \frac{1}{h} + \gamma \ln h$$

$$\mathrm{T}_3 = \frac{1}{2\mu_2}\frac{\partial ph}{\partial z} + \frac{\gamma}{4\mu_2}\frac{\partial ph^2}{\partial z}$$

$$\mathrm{K}_2 = \frac{T_2 - \epsilon T_3/\gamma}{\eta + \upsilon - \omega\epsilon/\gamma}, \quad K_3 = \frac{T_3}{\gamma} - \omega\frac{C}{\gamma}, \quad K_1 = K_2 \ln h_1 + K_3 - T_1$$

$$=\mathrm{U}_p - \cup, \quad \bar{K_3} = K_3 - \cup, \quad \bar{K_1} = K_1 - \cup$$

$$\mathrm{I(r,h}_p) = \int \frac{1}{r}(r - h_p)^{1/n+3}, \quad s_0 = \frac{h_p^2}{2}$$

$$\mathrm{s}_1 = \left(\frac{-1}{2\mu_1}\right)^{1/n}\frac{n}{n+1}\left(\frac{nh_1}{2n+1}(h_1 - h_p)^{1/n+2} - \frac{n^2}{(2n+1)(3n+1)}(h_1 - h_p)^{1/n+3}\right)$$

$$\mathrm{s}_2 = \frac{1}{2}\left(h_1^2 - h_p^2\right), \quad s_3 = \frac{1}{16\mu_2}\left(h^4 - h_1^4\right), \quad s_4 = \frac{1}{2}\left(h^2 \ln h - h_1^2 \ln h_1\right)$$

$$\mathrm{s}_5 = \frac{1}{4}\left(h_1^2 - h^2\right), \quad s_6 = \frac{1}{2}\left(h^2 - h_1^2\right)$$

$$\mathrm{M}_1 = \left(\frac{-1}{2\mu_1}\right)^{1/n}\frac{n}{n+1}(h_1 - h_p)^{1+1/n}, \quad M_2 = \frac{1}{4\mu_2}h_1^2, \quad M_3 = \left(\frac{-1}{2\mu_1}\right)^{1/n}(h_1 - h_p)^{1/n}$$

$$\mathrm{M}_4 = \frac{1}{2}h_1 - \beta\frac{1}{4}h_1^2, \quad M_5 = \frac{h}{2\mu_2} + \frac{\gamma}{4\mu_2}h^2, \quad M_6 = \eta + \upsilon - \omega\frac{\epsilon}{\gamma}$$

$$\mathrm{M}_7 = \frac{M_3}{M_6}, \quad M_8 = \frac{M_4}{M_6} - \frac{M_5\epsilon}{M_6\gamma}, \quad M_9 = M_9 - \omega M_8, \quad M_{10} = \omega M_7$$

$$\mathrm{M}_{11} = M_7 \ln h_1 - M_10 - M_1, \quad M_{12} = M_8 \ln h_1 + M_9 - M_2,$$

$$\mathrm{B}_1 = M_{11}(s_0 + s_2) + M_7(s_4 + s_5) - M_{10}s_6 + s_1, \quad B_2 = M_{12}(s_0 + s_2) + M_8(s_4 + s_5) + M_9 s_6 + s_3$$

$$\tau_y = -\frac{\partial p}{\partial z}\frac{h_p}{2}$$

$$\mathrm{B}_3 = \left(-2\frac{\tau_y}{h_p}\right)^{1/n-1}B_1 + B_2$$

A=$\left(\text{-16 }\frac{\mu_1}{h^4}\right)B_3$

$s_7 = \left(\frac{-1}{2\mu_2}\frac{\partial p}{\partial z}\right)^{1/n}\left(\frac{n}{n+1}\right)$

$s_8 = \frac{-1}{4\mu_2}\frac{\partial p}{\partial z}$

$T_4 = \frac{1}{D_m}\frac{\partial C}{\partial z}\left(\bar{K_1}(\right.$

$\left.4\text{- }\frac{h_p^2}{4}) + \frac{n^2 s_7}{(2n+1)(3n+1)}I(h_p,h_p)\right)$

$T_5 = \frac{1}{D_m}\frac{\partial C}{\partial z}\left(\frac{n^2 s_7}{(2n+1)(3n+1)}(h_1-h_p)^{1/n+3} - \frac{s_7}{2n+1}(\frac{n^2}{3n+1})I(h_1,h_p) - \frac{s_8 h_1^4}{16} - \right.$

$\left.\frac{K_2}{4}(h_1^2\ln h_1 - h_1^2) - \frac{\bar{K_3}h_1^2}{4} + \frac{\bar{K_1}h_1^2}{4}\right)$

$T_6 = \frac{h_1\partial C}{D_m\partial z}\left(\frac{s_8 h_1^3}{4} + K_2(\frac{h_1}{2}\ln h_1 - \frac{h_1}{4}) + \frac{\bar{K_3}}{2} - \frac{ns_7}{(2n+1)}(h_1-h_p)^{1/n+2} + \frac{ns_7}{(2n+1)}\frac{1}{h_1}\frac{n}{3n+1}(h_1-\right.$

$\left.h_p)^{1/n+3} - h_1\frac{\bar{K_1}}{2}\right)$

$T_7 = \frac{-h\partial C}{D_m\partial z}\left(\frac{s_8 h^3}{4} + K_2(\frac{h}{2}\ln h - \frac{h}{4}) + \frac{\bar{K_3}}{2}\right)$

G=$T_6 + T_7$, $\quad H = T_4 - G\ln h_p, \quad J = T_5 - I\ln h_1 + G\ln h_1 + H, \quad I = T_7$

$T_8 = \frac{\pi}{16}\frac{\hat{U}_p^2}{D_m}\frac{\partial C}{\partial z}h_p^4$

$T_9 = G_1 s_7 I_{21} - G_1 s_7 I_{22} + G_2 s_7 I_{23} + G s_7 I_{24} + H s_7 I_{25} + \bar{K_1}\left(G_1 I_{26} - G_1 I_{27} + G_2 I_{28} + G I_{29} + H I_{30}\right)$

$I_{21} = s\int_{h_p}^{h_1} r(r-h_p)^{2/n+4}dr, \quad I_{22} = \int_{h_p}^{h_1} I(r,h_p)r(r-h_p)^{1/n+1}rdr, \quad I_{23} = \int_{h_p}^{h_1} r^3(r-h_p)^{1/n+1}dr$

$I_{24} = \int_{h_p}^{h_1} r(r-h_p)^{1/n+1}(\ln r)dr, \quad I_{25} = \int_{h_p}^{h_1} r(r-h_p)^{1/n+1}dr, \quad I_{26} = \int_{h_p}^{h_1} r(r-h_p)^{1/n+3}dr$

$I_{27} = \int_{h_p}^{h_1} I(r,h_p)rdr, \quad I_{28} = \frac{1}{4}(h_1^4 - h_p^4), \quad I_{29} = \int_{h_p}^{h_1} r\ln r dr, \quad I_{30} = \frac{1}{2}(h_1^2 - h_p^2)$

$G_1 = \frac{1}{D_m}\frac{\partial C}{\partial z}\frac{n^2 s_7}{(1+2n)(1+3n)}, \quad G_2 = \frac{1}{D_m}\frac{\partial C}{\partial z}\frac{\bar{K_1}}{4}$

Working for equation (3.9) to (3.11)

Solving equation (3.9) to (3.11), we use the Herchel-Bulkely model shown below

$\tau = \tau_y + \left(-\mu_1\frac{\partial U_1}{\partial r}\right)^n$

Making $\frac{\partial U_1}{\partial r}$ the subject, the Casson model gives

$\frac{\partial U_1}{\partial r} = \left(\frac{1}{\mu_1}\right)^{1/n}\left(\tau - \tau_y\right)^{1/n}$

Using equation (3.10) on the above equation, we get

$\frac{\partial U_1}{\partial r} = \left(\frac{-1}{2\mu_1}\frac{\partial p}{\partial z}\right)^{1/n}\left(r - h_p\right)^{1/n}$

Hence equation (3.14) when the above equation is integrated once. Using the boundary condition (3.12) we get (3.13). Furthermore, intergrating twice on the equation (3.11), we

get equation (3.15)

Chapter 4 Appendix

$\omega_b = 2\pi f_b$

$\omega_p = 2\pi f_p$

$\tau_1 = p_n(t)p\prime(t)\frac{1}{n+1}\Bigg(n(r-k^2)^{1/n} - r(R-k^2)^{1/n+1} - \frac{n^2}{(1-n)}\frac{1}{r}(r-K^2)^{1/n-1} - \frac{r}{2}(R-k^2)^{1/n+1}\Bigg)$

$p_n(t) = p(t)^{1/n-1}, \quad p(t) = 2\big(1 + e\cos(\omega_p\frac{R_0^2}{D_m}t) + a_1\cos(\omega_b\frac{R_0^2}{D_m}t + \phi)\big), \quad p\prime(t) = \frac{\partial p(t)}{\partial t}$

$\sigma(t) = p\prime(t)\Big(p(t)\Big)^2/(n+1)$

$R_n = (R-k^2)^{1/n+1}$

$R_{n1} = \dfrac{n}{1-2n}$

$R_{n2} = \dfrac{n^2}{(1-2n)(1-3n)}$

$R_{n3} = \dfrac{n}{(2n-4n^2)}(R-k^2)^{1/n+1}$

$R_{n4} = \dfrac{n}{2-2n}$

$\mathrm{I}_1(r) = \int \frac{1}{r}(r-k^2)^{2/n-2}dr$

$A_i = \dfrac{\mu_i^2\int_0^1 rY(r)J_0(\mu_i r)dr}{(\mu_i^2+\beta^2)J_0^2(\mu_i)\int_0^1 rY(r)dr}$

$D_{mn}(t) = \int_0^t e^{-\lambda_j^2 s}\gamma(s)ds$

$\gamma(s) = \sum_{i=1}^{\infty} A_iA_j\int_0^t e^{-(\mu_i^2-\lambda_j^2)s}M_{nm}(s)ds + \sum_{i=1}^{\infty} A_iA_j\int_0^t \frac{1}{2}(J_0^2(\mu_i)+J_1^2(\mu_i))F_1(t)$

$M_{nm}(s) = \int_0^1 rw(r,s)J_0(\mu_i r)J_0(\mu_j r)dr$

$F_1(t) = \int_0^t k_1(s)ds = -2\dfrac{\sum_{i=1}^{\infty}\sum_{j=1}^{\infty} A_i(A_j^2/\lambda_j)e^{-\lambda_j^2 t}\int_0^t e^{-(\mu_i^2-\lambda_j^2)s}M_{nm}(s)dsJ_1(\lambda_j)}{\sum_{i=1}^{\infty}\sum_{j=1}^{\infty} A_j^2(A_i/\mu_i)J_1(\mu_i)e^{-\mu_i^2 t}(J_0^2(\mu_i)+J_1^2(\mu_i))}$

$\int_0^1 rw(t,r)f_0(r,t)dr = \dfrac{\sum_{i=0}^{\infty} A_ie^{-\mu_i^2 t}\int_0^1 rw(r,t)J_0(\mu_i r)dr}{\sum_{i=0}^{\infty}(A_i/\mu_i)e^{-\mu_i^2 t}J_1(\mu_i)}$

$$P(t) = -\sum_{j=0}^{\infty} A_kA_je^{-\beta_k^2 t}\int_0^t e^{-\beta_k^2 s}\left[b(s)M_{jk}(s) + \frac{K_1(s)}{2}(J_0^2(\lambda_j)+J_1^2(\lambda_j))\right]ds - \sum_{i=0}^{\infty} A_iA_ke^{-\mu_i^2 t}\frac{(J_0^2(\mu_i)+J_1^2(\mu_i))}{2}F_2(t)$$

$$F_2(t) = \frac{-\sum_{k=0}^{\infty}\sum_{j=0}^{\infty} A_j(A_k^2/\beta_k)e^{-\beta_k^2 t}\int_0^t e^{-\beta_k^2 s}\left[b(s)M_{jk}(s) + \frac{K_1(s)}{2}(J_0^2(\lambda_j)+J_1^2(\lambda_j))\right]dsJ_1(\beta_k)}{\sum_{k=0}^{\infty}\sum_{i=0}^{\infty} A_i(A_k^2/\mu_i)J_1(\mu_i)\frac{(J_0^2(\mu_i)+J_1^2(\mu_i))}{2}e^{-\mu_i^2 t}}$$

$M_{jk}(s) = \int_0^1 rw(s,r)J_0(\lambda_j r)J_0(\beta_k r)dr$

$b(t) = -\int_0^t e^{-\lambda_j^2(t-s)}\gamma(s)ds$

$$\gamma(s) = \sum_{i=1}^{\infty} A_i A_j \int_0^t e^{-(\mu_i^2 - \lambda_j^2)s} M_{nm}(s) ds + \sum_{i=1}^{\infty} A_i A_j \int_0^t \frac{1}{2}(J_0^2(\mu_i) + J_1^2(\mu_i)) F_1(t)$$

$$2\int_0^1 rw(t,r) f_1(r,t) dr = \frac{-2\sum_{k=0}^{\infty} A_k e^{-\lambda_j^2 t} D_{mn \int_0^1 rw(t,r) f_1(r,t) dr}(t) \int_0^1 rw(t,r) J_0(\lambda_j r) dr}{\sum_{i=0}^{\infty} (A_i/\mu_i) e^{-\mu_i^2 t} J_1(\mu_i)}$$